Master thesis

Influence of proteasome inhibitor bortezomib on cell cycle distribution of human chondrosarcoma cells

submitted by

Philipp-Maximilian Umland

For the degree of

Doctor medicinae universiae

(Dr. med. univ.)

At the

Medical University of Graz (AUT)

Performed at

Department of Orthopedics and Trauma

Supervised by

Priv.-Doz.in Mag.a rer. nat. Dr.in scient. med. Birgit Lohberger
Univ. Prof. Dr. Andreas Leithner

Graz, 15.09.2017

Declaration

I hereby declare that I have authored this thesis independently, that I have not used other than the declared sources / resources, and that I have explicitly marked all material which has been quoted either literally or by content from the used sources.

Graz, 15.09.2017 *Philipp-Maximilian Umland eh.*

Acknowledgement

First, I would like to thank my supervisor Dr. Birgit Lohberger, for the opportunity to write this thesis. I am very grateful for her support, helpful advices and her engagement during the whole time of the study. Special thanks go to Heike Kaltenegger and Nicole Stündl for their patience and assistance during my first steps into laboratory work and throughout the study.

My greatest appreciation goes to my parents Daniela Felicitas and Klaus-Henning Umland who supported me in every possible way to have worriless student days.

Zusammenfassung

Das Chondrosarkom ist durch eine sehr schlechte Ansprechrate bezüglich herkömmlicher Chemo- und Strahlentherapie charakterisiert. Als zweithäufigstes Knochensarkom hat es eine sehr geringe Überlebensrate, insbesondere bei Auftreten von Lungenmetastasen. Aus diesem Grund beschäftigt sich die aktuelle Forschung intensiv mit der Entdeckung und Entwicklung neuer Wege und Therapeutika, um das Chondrosarkom zu besiegen. Heutzutage beschäftigen sich viele Studien mit der Effektivität von Proteasomen Inhibitoren (Bortezomib) auf verschiedenste Tumorarten. Bezüglich Bortezomib gibt es auch schon vielversprechende Ergebnisse im Bereich solider Tumore wie beispielsweise das Ovarialkarzinom, Prostatakarzinom, Ewing Sarkom oder auch das Osteosarkom. Dennoch gibt es nur sehr wenige Daten bezüglich der Effektivität auf das Chondrosarkom. Unsere Studie soll ein kleiner Beitrag sein, um diese Lücke zu schließen. Unsere Ergebnisse zeigten, dass Bortezomib die Zellzahl und Zellproliferation der Chondrosarkomzelllinie SW-1353 zeitabhängig und konzentrationsabhängig verringert. Desweiteren zeigte die FACS Analyse mit dem Einsatz von Bortezomib einen signifikanten G2/M Arrest. Darauffolgend wurde eine quantitative Real-time Polymerasekettenreaktion durchgeführt, um den Effekt auf das Genexpressionslevel von CCNA, CCNB, CDK1, CDK2 und cdc25 zu analysieren. Dabei war eine generelle Abnahme zu verzeichnen.

All diese Ergebnisse unterstützen den Gedanken, dass Bortezomib als Inhibitor des Zellzyklus Fortschrittes fungiert, indem es in das Cyclin/CDK System eingreift und damit die Proliferation einschränkt. Wenn diese und bereits bekannte Effekte auch in Tierversuchen nachweisbar sind, könnte Bortezomib ein nützliches zukünftiges Therapeutikum in der Therapie des Chondrosarkoms sein.

Abstract

Chondrosarcoma, the second most common bone sarcoma, is characterized by a very low respond to traditional chemo- and radiation therapy and a bad survival rate especially with the occurrence of lung metastases. Therefore, the current research is meticulously focused on the finding and the development of new trials and new therapeutic substances to defeat chondrosarcoma. A lot of studies today deal with the efficiency of proteasome-inhibitors (bortezomib) to various types of cancer. According to bortezomib, there are promising results for the efficiency against solid tumors like the ovarian tumor, prostate cancer, Ewing´s sarcoma and osteosarcoma, but only very limited data about the efficiency to chondrosarcoma. Therefore, our study is a little contribution to close this gap. Our findings showed that Bortezomib could decrease the cell viability and proliferation of chondrosarcoma cell line SW-1353 in time- and dose-dependent manner. Furthermore, FACS analyses revealed a significant G2/M arrest by using bortezomib. In addition, a quantitative real-time Polymerase-Chain-Reaction was performed to analyze the efficacy to the gene expression levels of CCNA, CCNB, CDK1 and CDK2. Therefore, a general decrease was determinable.

All these results support the idea that bortezomib functions as an inhibitor of cell cycle progress by intervening in the cyclin/CDK system and therefore it can limit the proliferation. When these and already known effects can also be demonstrated in animal experiments, bortezomib might be a useful chemical drug for the future therapy of chondrosarcoma.

Contents

Abbreviation

A

ATM	Ataxia telangiectasia mutated
ATP	Adenosine Tri-Phosphate

C

Cdc2	Cell division cycle 2
Cdc25	Cell division cycle 25
CI	Cell Index
CDK	Cyclin-dependent kinase
CHK1	Cell cycle checkpoint kinase 1
Cy-2	Cyanin-2

D

DAPI	Diamidino phenylindole
DNA	Deoxyribonucleic acid

E

EDTA	Ethylenediaminetetraacetic acid
ERK-Kinase	Extracellular-signal regulated kinase

F

FSC	Forward scatter

G

g	gravitational force
G-Phase	Gap-phase

H

h	hour
HDM2	Human double minute 2

I

IC25	Inhibitory concentration 25
IC50	Inhibitory concentration 50

L

l	Liter

M

MgCl2	Magnesium chloride
Mg	milligram
min	minute
M-phase	Mitosis-phase
MTS	[3-(4,5-dimethylthiazol-2-yl)-5-(3-carboxymethoxyphenyl)-2-(4-sulfopphenyl)-2H-tetrazolium] inner salt

N

NADP	nicotinamide adenine dinucleotide phosphate
nM	nanomole
nm	nanometer

O

OD	Optical density

P

PI	Propidium iodide
PCR	Polymerase chain reaction
PES	Phenazine ethosulfate

Q

qRT-PCR	Quantitative Real-Time PCR

R

RAS	Ratsarcoma
Rb	Retinoblastoma
RIN	RNA Integrity number
RNA	Ribonucleic acid
Rpm	Rounds per minute

S

S-Phase	Synthesis-phase
SSC	Sideward scatter
STR	Short tandem repeats

µ

µl	microliter
µg	microgram

V

VC	Vehicle control

Index of Figures

Index of Tables

1 Introduction

Tumor-diseases are increasingly relevant in global medicine. In the statistic of the causes of death, cancer takes second place after cardiovascular diseases. The incidence of malignant tumors is at approximately 500 per 100.000 people per year. [1] Although malignant bone tumors with an incidence of 1-2 per 100.000 are rare, the following thesis deals with chondrosarcoma, the second most common malignant bone tumor, on the level of basic research. [2] [3]

1.1 Bone Tumors

Neoplasia of the skeletal system can be divided into primary and secondary bone tumors. While primary malignant tumors are rare, benignant tumors are 3 - 4 times and metastasis are 2.5 times more frequently. [4]

Over 50 percent of the primary malignant tumors manifest themselves in children and adolescence, especially the Ewing´s sarcoma and osteosarcoma. [4] An exception is provided by chondrosarcoma, which occurs in adults older than thirty. [5]

Malignant neoplasia of the bone is based on neoplastic osteogenic mesenchyme cells, which can differentiate in an osteoblastic, chondroblastic, or fibroblastic way. [4]

According to the diversity of differentiation, the World Health Organisation classified over 60 forms of bone tumors after the predominant tissue. [4]

In general, the precise aetiology is still unknown. Even though there are some genetic aspects, which lead to a dysfunction of cell cycle control. [6] This correlation will be explained later. Initially, a detailed description of chondrosarcoma is necessary.

1.2 Chondrosarcoma

Chondrosarcoma, as already mentioned, are the second most common sarcoma of the bone. [3] It can be classified into the common primary chondrosarcoma and the less common de-differentiated, clear-cell, and mesenchymal subtypes. [7]

There are also secondary variants. These chondrosarcoma have their origin in benign precursors, like osteochondroma or enchondroma. [7]

The peak of incidence is between 50-70 years of age and a little bit more frequent in the male gender. [7]

Predilection sites are the bones of the pelvis, especially the Ileum. Moreover, the proximal and distal femur, proximal humerus, ribs and proximal tibia are frequently targeted. (Figure 1) [7]

Tumor spread is hematogen and metastases can be found in the lung. Until today there have also been three cases of metastasis to the thyroid gland. [8][9]

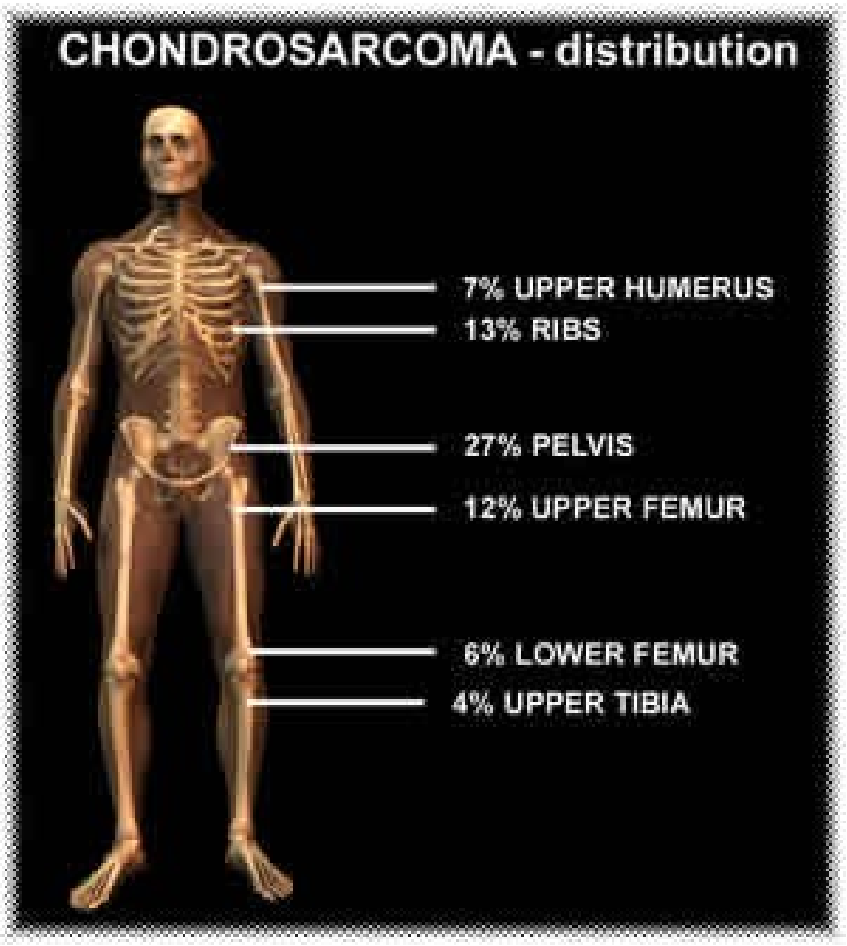

Figure 1: Distribution of chondrosarcoma

(https://www.joinclinicaltrials.com/blog/wp-content/uploads/2012/05/Chondrosarcoma.jpg)

The basic substance of chondrosarcoma is the hyaline cartilage. There are also a lot of tumors showing calcification and bone structure at histological level. Bone structure itself is not produced by chondrocytes, but seems to be a result of endochondral ossification. [10] Beside calcification and bone structure, high-grade chondrosarcoma can also appear with haemorrhage and necrosis (Figure 2). [10]

Depending on the grade of chondrosarcoma, the histological level of chondrocytes shows a wide diversity of cell nuclear atypia. Above all, cell enlargement, mitotic rate and karyotypes are conspicuous. [10]

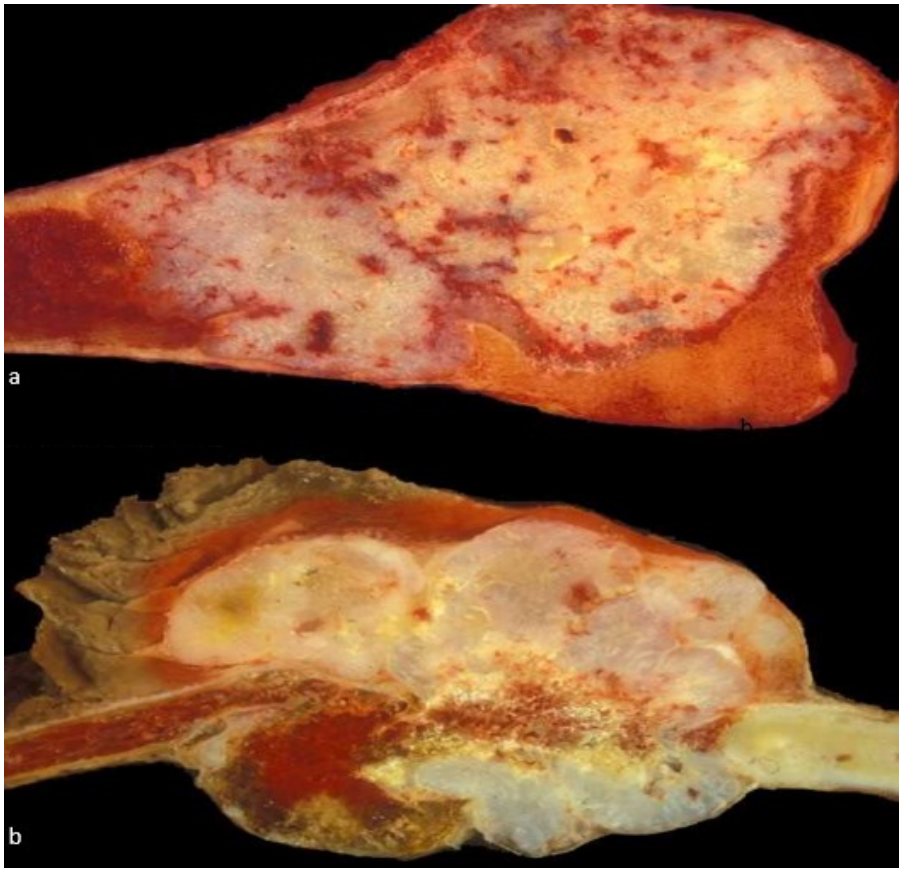

Figure 2: Chondrosarcoma of femur (a) / rib (b), white-yellow part: proliferated chondrocytes with necrotic areas, red: haemorrhage

(http://www.pathpedia.com/education/eatlas/grosspathology/bone/Images.aspx?5)

To diagnose chondrosarcoma the anamnesis is helpful. Patients with chondrosarcoma report pain and swelling lasting for month or even years. Furthermore, radiological examination is expedient. X-ray shows normally fusiform expansion and the cortex increases in thickness. Despite increasing thickness, radiolucency is high and there are signs of mineralization. An attacked cortex is apparent (Figure 3).

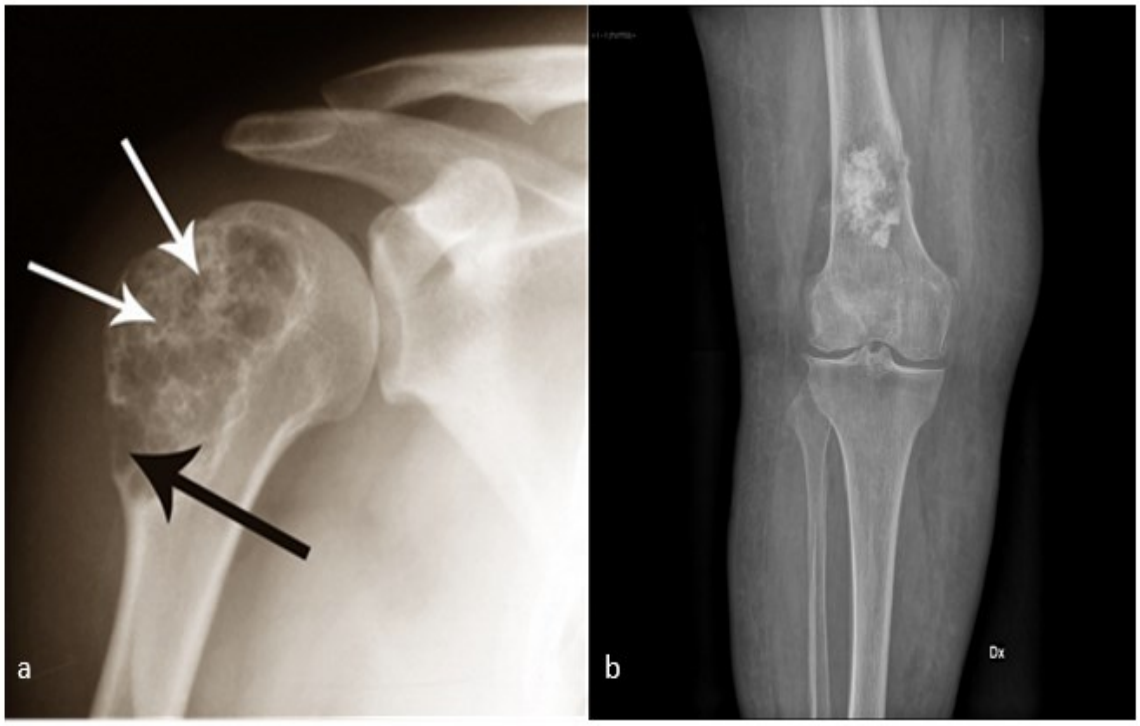

Figure 3: a) Chondrosarcoma of the proximal humerus, white arrows: signs of mineralization, black arrow: osteolytic area b) Chondrosarcoma of distal femur: osteolysis and cortical extension

((a) http://mddk.com/chondrosarcoma.html, (b) https://radiopaedia.org/cases/chondrosarcoma-4)

Sometimes magnetic resonance imaging is useful to clarify the tumor expansion itself and the expansion of soft tissue infestation. [7]

The primary therapy is complete surgical tumor resection. The efficiency of adjuvant chemotherapy has not yet been adequately proven. Chondrosarcoma also show little radio sensitivity. For this reason, radiotherapy is just used in some cases of inoperability. [9]

The prognosis is strongly influenced by the histological grade. Grade 1 implicates a tumor without any tendency to metastasis, therefore the five-year survival rate is 89%. With grade 2 and 3 metastasis is more frequent and the five-year survival rate falls to 53%. [7]

1.3 The Cell Cycle

The cell cycle is one of the central features in the understanding of cancer development. Uncontrolled growth of cancer cells is strongly related to typical mutations of the cell cycle

regulating genes. There are two groups of important genes, the proto-oncogenes and tumor suppressor genes. Proto-oncogenes are genes, which promote cell growth and lead to uncontrolled cell proliferation in case of mutation. [11] In this context, Ras- (Rat sarcoma), HDM2- (Human double minute 2), MYC- and for our study more important the genes of cyclins should be mentioned. In contrast tumor suppressor genes, like the Rb- (Retinoblastoma), P53- and P21 gene, encode proteins, which stop the progress of growing. Therefore, the loss of function also results in excessive proliferation. In general mutations of proto-oncogenes or tumor suppressor genes lead to critical concentration or dysfunction of proteins, which are involved in the management of the cell cycle progress.[11]

The cell cycle itself is composed of two main parts, the M-phase and the interphase. [12]

The M-phase lasts around one hour and can be divided in prophase, metaphase, anaphase, telophase, and cytokinesis. [11] [12] In this work, a detailed description of the individual phases is omitted, but it is important to know that a segregation of chromosomes takes place and that two daughter cells are formed with 46 one-chromatid-chromosomes during the M-phase. As a result, the DNA content of the cell is halved after Mitosis. [11] The interphase takes around 23 hours and is organised in three various parts. During G1-phase, the cell grows and prepares for DNA-replication, which takes place in the S-phase. In relation to the replication of DNA, the old DNA content of 46 two-chromatid-chromosomes is recovered. The G2-phase, as the third part of the interphase, prepares for the next M-phase and controls, if the DNA-replication was right. If there are any mistakes, the cell is able to start apoptosis. [13]

As a marginal note, the cell is also able to leave the cycle between the G1 and S-phase. This phase is called G0. In this phase cell division is inactive, but can be resumed when there are better conditions. [12]

Obviously, the transitions between single phases are strictly controlled by molecular checkpoints to avoid cell damage. The most important ones are the G1/S checkpoint and the G2/M checkpoint. In the following section, we want to focus on these two points, although there are some more points of control during the M- and S-phase.

There is also a complexity of molecular switches, which work all together as a closely linked network to conquer the checkpoints, so that it is not possible to emphasize all of them in the theoretical part of this thesis. For our research, the cyclin/ cyclin-dependent kinases system is particularly important and will be explained in the following chapter.

Cyclin-dependent kinases (CDK) involve various groups of serine and threonine protein kinases. These kinases are activated at different points during the cell cycle and phosphorylate specific proteins, whereby the activation is triggered. [14]

Activated proteins are now able to work on cell cycle progress. The concentration of CDK during the cell cycle is very solid, but the activity strongly depends on their cyclin-activators which fluctuate referring to different cycle phases (Figure 4).

Therefore, CDK has also a periodically activation. [15]

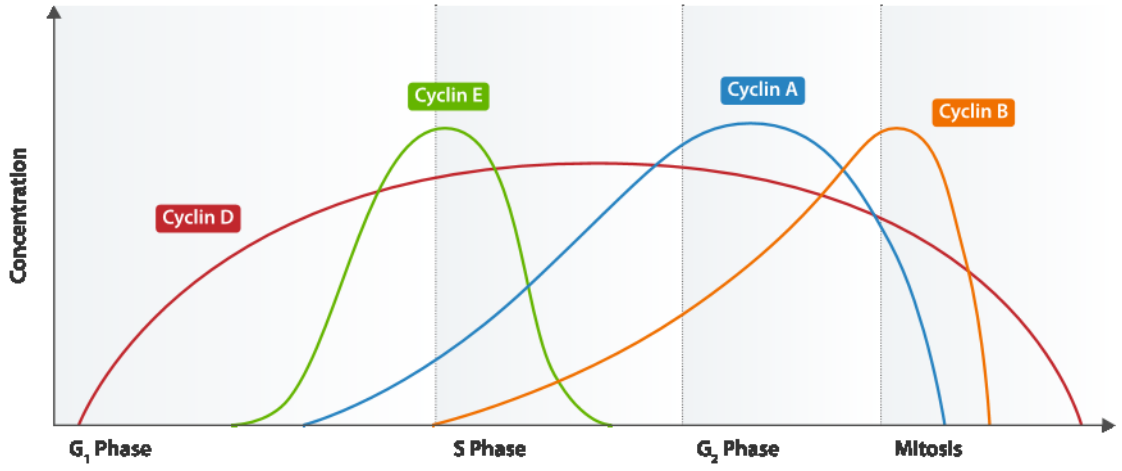

Figure 4: Cycle dependent concentrations of cyclins

(https://en.wikipedia.org/wiki/Cyclin_E#/media/File:Cyclin_Expression.svg)

Cyclins are proteins with a cyclic expression, as already mentioned above, and can be divided into G1-phase- and M-phase-cyclins. G1-Phase cyclins are necessary to pass G1/S-checkpoint, especially cyclin D and cyclin E. M-phase-cyclins, mainly cyclin A and cyclin B, are indispensable for G2/M-checkpoint. [11]

Except for cyclin D, which has a constant expression during the cell cycle, every cyclin is removed after fulfilling its specific function. Therefore, the cyclin is marked by the ubiquitin-system to be resolved directly for the proteasome. [11]

For a precise understanding Figure 5 shows the detailed relations between the specific cyclins and their cyclin-dependent kinases.

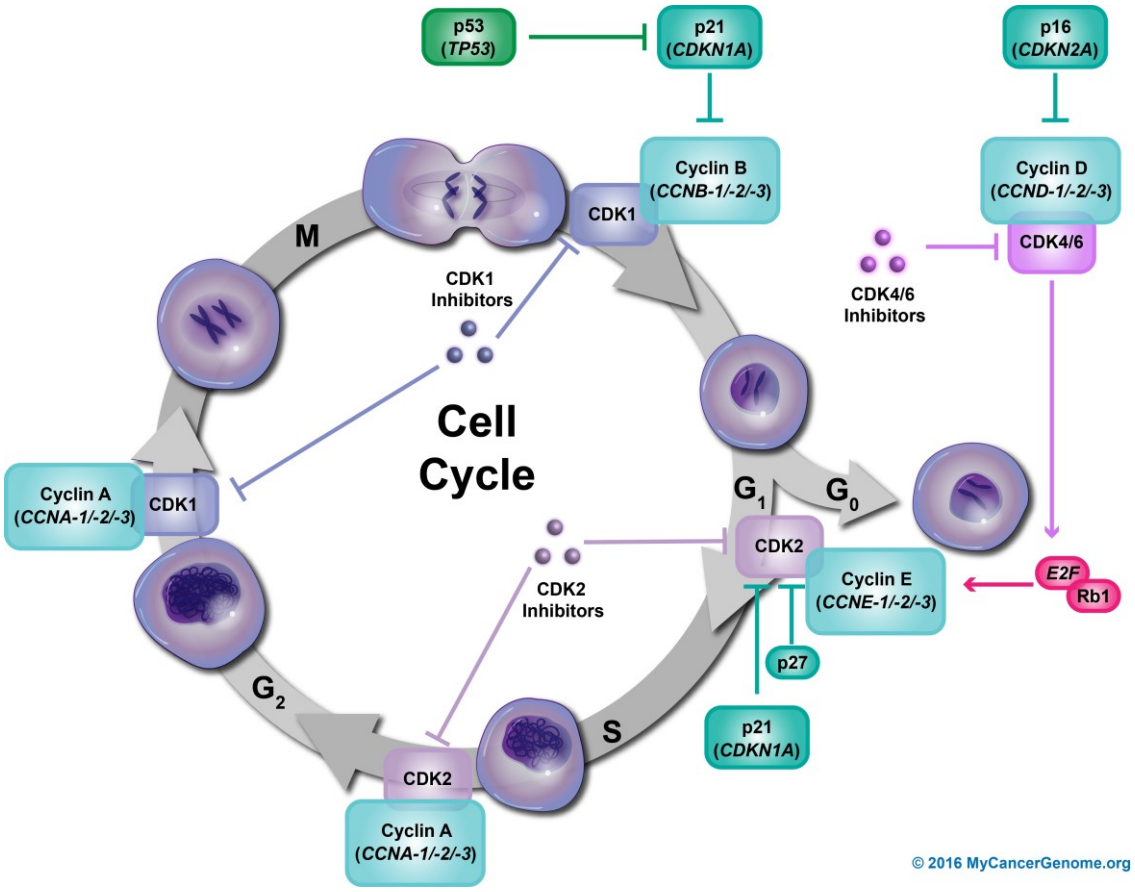

Figure 5: Cyclin-CDK-System during the progress of cell cycle

(https://www.mycancergenome.org/content/molecular-medicine/pathways/cell-cycle-control-DNA-damage)

The active CDK during the cell cycle are CDK4, CDK6, CDK2, and CDK1.

CDK4 and CDK6 interact with Cyclin D and represent an important active complex for entering G1 phase. [16]

Furthermore, the Cyclin E/CDK2 complex is included in the regulation of progression from G1 into S-phase. [17]

Another complex is formed by Cyclin A and CDK2 and is needed during S-phase. [18] In addition, there is an important complex in the late G2 and early M-phase, called cyclin A/CDK1. Finally, M-phase is also regulated by Cyclin B/CDK1 complex. [19]

One of the most famous targets of activated CDK is retinoblastoma tumor suppressor gene (Rb), primarily influenced by CDK4 and CDK 6. In activated conditions, the Rb-protein makes sure that a strongly needed transcription factor is blocked. This transcription factor is called E2F and releases transcription of S-phase genes. When CDK4 and CDK6 are active, Rb-protein is phosphorylated and loses its function. Consequently, E2F is no longer captivated and the cell goes from G1 to S-phase. [11]

S-phase gene activation also includes the production of cdc25 and other cyclins, like cyclin A/E which are needed for subsequent processes. [20] Cyclin A/E activated CDK2 is furthermore important for S-phase progress, like chromosome condensation or initiation of DNA-replication. [21] [22]
Cyclin A also activates CDK1 in late G2 to which reference has already been made.
Cdc25 (Cell division cycle 25) is another activator for CDK by dephosphorylation and consists of three different subtypes cdc25A, cdc25B and cdc25C. Cdc25A takes part in the transition of G1 to S-phase. Cdc25B has compulsory attendance during S-phase and cdc25B is important for the activation of cyclin B/CDK1 complex during mitosis. Uncontrolled cdc25 expression is a key for tumor development. [23]

To understand Figure 5 completely, it is necessary to state that CDK is not only influenced or controlled by cyclins and cdc25. Other influence factors which are shown in Figure 5 can be summarized as CDK inhibitors (CDI). Important CDI are P16, P21 and P27.

The P16 family includes proteins, that are specific inhibitors of CDK4 and CDK6.
The main representative Protein P16 competes with cyclin D for the active side of CDK and inhibits the phosphorylation of Rb. Consequently, the progress to S-phase fails.
Proteins of the P21-family (P21/P27) have a small influence on CDK4 and CDK6 but are more integrated in the inhibition of CDK2. For this reason, the p21-family inhibits G1-phase as well as the transition from G2 to M-phase.
Finally, we would like to clarify the meaning of the protein P53. P53 is worldwide known as the guardian of the genome. It is responsible for stopping cell division and is also able to introduce apoptosis, when DNA is damaged. With increasing DNA damage, the cell expresses more P53 and therefore cell cycle arrest or even apoptosis is introduced by two important mechanisms. P53 induces the expression of P21 for cell cycle arrest or BAX genes in case of apoptosis. [11]

After the explanation of the relevant cell cycle control mechanisms, we want to give a short insight in the function of Bortezomib. Under the influence of Bortezomib we analysed gene expression of cyclin B, cdc25, CDK1 and CDK2.

1.4 The proteasome and the influence of bortezomib

Bortezomib is a proteasome inhibitor. The proteasome itself works as an ATP- dependent protease-complex inside the cytosol and has a central part in the degradation of proteins. On the one hand, it helps to eliminate wrongly folded proteins and on the other hand the half-time period of some proteins, that change their concentration during cell progress very quickly, is reduced by the proteasome activity. In our case the focus is put on the cyclin and cdc25 degradation during various phases of the cell cycle.

The proteasome consists of a hollow cylinder, the so-called 20S-core-proteasome, and the so-called 19S-cap. The 20S-core-proteasome comprises a lot of individual proteases with its active center in the inside of the hollow cylinder, so that the cell is protected of uncontrolled proteolysis activity. The 19S-cap is the marginal structure of the proteasome. This protein-complex consists of an unfoldase-group, often called AAA-proteins. This structure enables the proteasome to bind a specific protein for degradation. By an ATP-dependent hydrolysis the protein is in the middle of proteasome and gets in contact with proteases of 20S-core-proteasome.

To bind a protein, it is essential, that the protein is marked by Ubiquitin-proteins before (Figure 6).

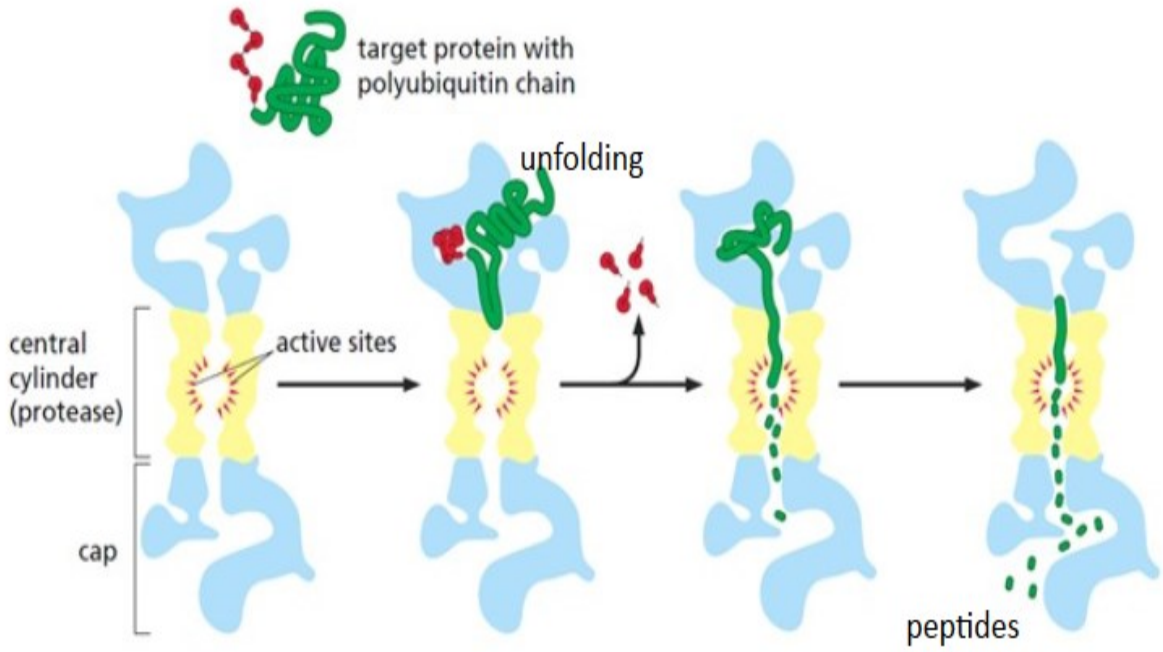

Figure 6: Proteasome structure and the principle of binding target proteins

(Alberts et al., Molecular Biology of The Cell, 6th Edition, 2015, p. 358)

Ubiquitin-proteins are free or connected proteins in the cytosol and get activated by a Ubiquitin-activating-enzyme E1. This is also an ATP-dependent step. In the following, the E1-binded-activated Ubiquitin is transmitted to a group of Ubiquitin-conjugating-enzymes E2. E2 works together with a helper protein E3 as a Ubiquitin-ligase. Thereby, the E3 component binds a specific signal of the protein, that must be degraded. In addition, E3 helps E2 with transmission of Ubiquitin to a specific lysine rest of the targeted protein.
In this way, a polyubiquitin-chain is constructed and ready for binding to specific receptors of 19S-cap.
Of course, there are different components of E2/E3 and different signals for protein degradation, so that a specific removing of proteins is possible. [24]
Bortezomib, a pyrimidine-carboxamide containing boron, inhibits the 26S proteasome (19S +20S) and therefore the Ubiquitin-degradation-system loses its function (Figure 7).

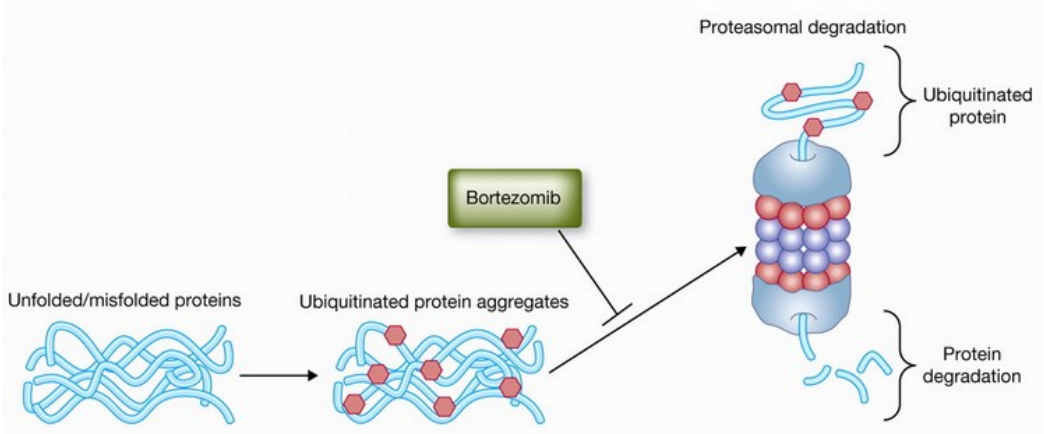

Figure 7: The influence of bortezomib: bortezomib inhibits the proteasome and therefore protein degradation is not possible

(http://mct.aacrjournals.org/content/molcanther/10/11/2034/F2.medium.gif)

The result is a change of the cell cycle regulating protein-concentrations and transcription factors. Furthermore, the cell-growing, angiogenesis, cell to cell interaction and metastasis are inhibited. [25]
Bortezomib has been already approved for the treatment of multiple myeloma and mantle cell lymphoma under the trade name Velcade®. There are also some indications for the efficiency against solid tumors like the ovarian tumor, prostate cancer, Ewing´s sarcoma, osteosarcoma and some squamous cell cancer types of the head and neck. [26] However, the complete effect mechanism is still unknown, although we have isolated references like

inactivation of Stat3 signaling [27] or stimulation ERK- (Extracellular-signal Regulated Kinases) phosphorylation. [28]

1.5 Study design

Our study supports the scientific research of bortezomib efficiency to chondrosarcoma cells. We analysed the proliferation of human chondrosarcoma cells and human chondrocytes with due regard to the influence of the proteasome-inhibitor bortezomib on the cell cycle. Therefore, this thesis gathers information about the following aspects:

- **Characterisation of human chondrocytes and chondrosarcoma cell line SW-1353**. In this context, we performed a short-tandem-repeat analysis to have a DNA-based evidence. Furthermore, we performed a vimentin-DAPI immunofluorescence imaging to prove the mesenchymal origin.
- **Cell viability** was controlled by using MTS- cell viability assay (Promega).
- **Quantification of adherent cell proliferation and viability in real time** was checked by using the xCELLingence RD device system (ACEA Biosciences).
- **Changes in the distribution of cell cycle phases under the influence of bortezomib** were supervised by using the BD FACSCalibur™ system (BD Biosciences)
- **Changes in the gene expression levels of CCNA, CCNB, CDK1, CDK2, cdc25** were observed by the technique of Real – time quantitative Polymerase-Chain-Reaction

2 Materials and Methods

2.1 Cell lines and cell culture conditions

For our study, we bought human chondrocytes (HC-C15/C23) from the company Cell Applications (San Diego, CA). These chondrocytes were compared with the immortal tumor cell line SW-1353 (CLS, Eppelheim, Germany).

Human chondrocytes were isolated from normal healthy articular cartilage of a 65 years old caucasian male. [29] Whereas, the SW-1353 cell line was used first by A. Leibovitz at the Scott and White Clinic, Texas, in 1977 and was isolated from a primary grade II chondrosarcoma of the right humerus. The patient herself was 72 years old and a female caucasian. [30]

In general, our used cells were cultured in T175 flasks in an incubator at 37° C and a CO_2 atmosphere of 5 %. The chosen culture medium was Dulbecco´s modified

Eagle medium with high glucose DMEM/F-12 (GIBCO®, Invitrogen, Darmstadt, Germany). The medium was also modified with amphotericin B [0.1%] (PAA Laboratory, Pasching, Austria), L-glutamine [1.0%] (Gibco®, life technologies™), penicillin streptomycin [1%] (Gibco®, life technologies™) and foetal bovine serum [10%] (Gibco®, life technologies™). (Table 1)

DMEM-F12 m. PR, Gibco, 21041	500 ml
Foetal Bovine Serum, Gibco, 10270-106	50 ml
Penicillin Streptomycin, Gibco, 15140	5.5 ml
Amphotericin B, PAA, P11-001	0.55ml
L-Glutamine, Gibco, 25030	5.5 ml

Table 1: Culture medium

After reaching a confluence of around 90 %, cells were sub-cultured with Accutase® (Innovative Cell Technologies, San Diego, CA). After all, cells were used for the following methods. First, we did a Vimentin - 4´, 6 - diamidino - 2 - phenylindole (DAPI) Immunofluorescence and a Short-Tandem-Repeats-Analysis (STR) for identifying our cell lines.

2.2 Vimentin – DAPI Immunofluorescence

We performed the vimentin – DAPI - Immunofluorescence to confirm the mesenchymal origin of HC and SW-1353. Vimentin is an intermediate filament and is a part of the cytoskeleton structure of vertebrate cells. There are five classes of intermediate filaments, whereby vimentin belongs to class III and characterizes mesenchymal cells. [31]
For the evidence of vimentin, we used the principle of indirect immunofluorescence.
The cells were first tagged with a monoclonal anti-vimentin antibody (Dako, Santa Clara, CA). The Anti-vimentin antibody was bound at a specific part of the constant region by a second cyanin-2 conjugated goat anti-mouse antibody (Jackson ImmunoResearch, West Grove, PA). Cyanin - 2 (cy-2) is a green fluorescent probe. Therefore, it enabled us to visualize generated complexes with a fluorescence microscope.
In addition to the vimentin dye, we also did a nucleus counterstaining by 4´, 6 – diamidino -2 - phenylindole (DAPI). DAPI is a blue fluorescent probe and intercalates with the DNA.

2.2.1 Protocol

Initially, we prepared our used antibodies. The vimentin antibody [156 mg/L] (Dako) was diluted [1:100] with phosphate-buffered saline 1x (PBS; Gibco®, life technologies™) containing 1% bovine serum albumin (BSA) and 0.3% Triton™ X-100 (Sigma Aldrich). The second cy - 2 conjugated goat anti-mouse antibody [1.5 mg/ml] was diluted with the same antibody diluent and dilution factor.
We also used an unspecific immunoglobulin G (IgG) as a negative control.

The primary chondrocytes and SW-1353 cells were plated into chamber slides with 3000 cells/well. After overnight incubation, the cells were washed with PBS 1x and dried for 2 hours at room temperature and after all dried chamber slides were added to a -20° fridge overnight.
In a next step, the cells were fixed using 4 % paraformaldehyde for 10 minutes and the fixed cells were washed with PBS 1x.
To reduce background measurement during the following image recording, we also applied Ultra Vision Protein Block (Thermo Fisher Scientific, Waltham, MA) to our cells for 5 minutes. Therefore, we could reduce unspecific protein bindings.
After finishing all the necessary, we were now ready to use our antibodies.

The diluent containing the vimentin antibody was added to chamber three and four (200 µl) and was incubated for 30 minutes at room temperature. We pipetted our unspecific IgG in chamber one and the pure antibody diluent in chamber two. (Figure 8)

Chamber 1	Chamber 2	Chamber 3	Chamber 4
IgG (1:100) + Goat-anti-mouse Antibody	Antibody-diluent + Goat-anti-mouse Antibody	Vimentin-Antibody + Goat-anti-mouse Antibody	Vimentin-Antibody + Goat-anti-mouse Antibody

Table 2: Scheme of chamberslide in relation to the instructed antibodies

After exposure time of 30 minutes, washing steps with PBS 1x (3 x5 min) were conducted. Afterwards the cy-2 conjugated goat anti-mouse antibody was added to all chambers (200 µl/well). We added another incubation time for 30 minutes protected from light and some more washing steps with PBS 1x (3 x 5 min).
The last step was to cover our slides with DAPI for counterstaining. Therefore, we used Vectashield Mounting Medium purchased from Vector Laboratories (Burlingame, CA).
The cells were saved in the dark and viewed with a Confocal LSM 510 META Fluorescence Microscope (Zeiss, Vienna, Austria). ZEN 2009 software (Zeiss) was used to take and process the images.

2.3 STR – Analysis

Short - Tandem - Repeats are repetitive sequences of DNA inside the introns of a gene. These tandem repeats consist of two to seven pairs of nucleotides and can be used as a specific marker for identifying cell types. Therefore, every cell type has a specific number of tandem repeats, which are called STR- Loci. [32] Accordingly, these STR-Loci can be analyzed by different technologies. In our case, we used a Polymerase-Chain-Reaction (PCR)-based short tandem repeat analysis for verifying SW-1353 using a Powerplex16 System Kit (Promega, Mannheim, Germany).

2.3.1 Protocol

For the STR-Analysis we had to isolate DNA of SW-1353. Therefore, we used the QIAamp DNA Mini Kit from Qiagen (Hilden, Germany). According to the manual, we transferred 5 x 10^6 of our harvested cells to a 1.5 ml microcentrifuge tube and centrifuged for 5 min at 300 x g. The supernatant was discarded and the pellet was solved in PBS to a final volume of 200 µl. In the next step, we added 20 µl QIAGEN protease and 200 µl buffer AL. Afterwards, the sample was vortexed for 15 seconds and incubated at 56°C for 10 minutes.

After a light centrifugation, the sample was processed with 200 µl ethanol (96-100%). The sample was vortexed and centrifugated again.

This mixture was applied to the QIAamp Mini spin column and we did a centrifugation at 6000 x g for one minute. The centrifugate effluent was discarded and the tube containing the filtrate was put in a clean two milliliter collection tube.

In the following step, we added 500 µl buffer AW1 and centrifugated at 6000 x g for one minute and put the spin column to another clean 2 ml collection tube. The filtrate was discarded again.

We opened the spin column again and added 500 µl buffer AW2. The next centrifugation was performed at 20,000 x g for three minutes. We changed the collection tube again and started another centrifugation at 20,000 x g for one minute.

The spin column was now placed in a 1.5 ml microcentrifuge tube and treated with 200 µl buffer AE. We had incubation at room temperature for one minute and centrifugated for a last time at 6000 x g for one minute.

After all, DNA was isolated and we checked the purity with the NanoDrop system (eqLab Biotechnologie GmbH, Erlangen, German). The optical density of our samples was red at 260 nm and 280 nm.

We were not able to perform the STR-Analysis in our laboratory. For this reason, we sent our sample to an external company (Institute of human genetics, Medical University of Graz) where PCR-based short tandem repeat analysis for verifying SW-1353 using a Powerplex16 System Kit was performed.

2.4 Cell viability assay

Our first experiment correlated with bortezomib was the CellTiter 96 AQueous One Solution Cell Proliferation Assay (Promega, Madison, MI). We used this assay to study the influence of bortezomib to the viability of primary chondrocytes and SW-1353. Therefore, the cells were treated by different concentrations of bortezomib and effects were measured by a colorimetric method.

The assay´s core is a redox reaction which converts the compound of [3-(4,5-dimethylthiazol-2-yl)-5-(3-carboxymethoxyphenyl)-2-(4-sulfopphenyl)-2H-tetrazolium inner salt (MTS) and phenazine ethosulfate (PES) (Owen`s reagent) to a brown-colored formazan product (Figure 8).

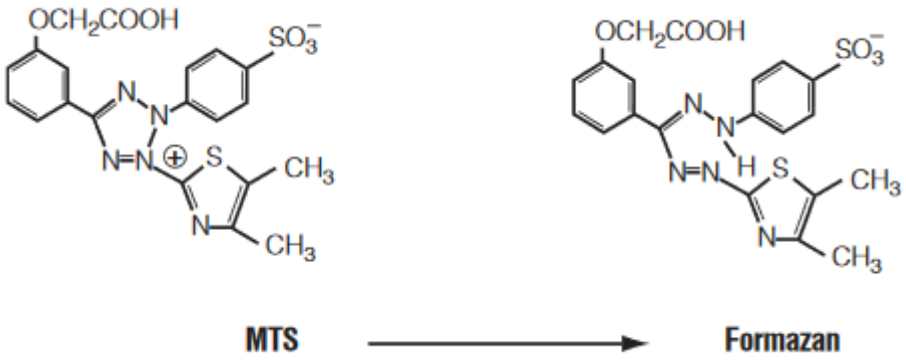

Figure 8: Chemical reaction of MTS tetrazolium to its formazan product

(https://at.promega.com/-/media/files/resources/protocols/technical-bulletins/0/celltiter-96-aqueous-one-solution-cell-proliferation-assay-system-protocol.pdf)

This reaction is supported by the reduction of nicotinamide adenine dinucleotide phosphate (NADP). NADP is produced by dehydrogenase enzymes in metabolically active cells and functions as metabolic marker. Consequently, the measured conversion of MTS depends on the number of living cells which determine the NADP rate. [33]

2.4.1 Protocol

Primary chondrocytes and SW-1353 cells were plated into 96-well- plates. Three plates were used for each cell culture to show the effects of bortezomib at three various time points (24/48/72 hours). 6 x 10^3 cells per well were seeded and the plates were incubated overnight. The next day, cells were treated with bortezomib (0 nm, 0.5 nm, 1 nm, 2.5 nm, 5

nm, 10 nm, 25 nm, 50 nm, 100 nm, 250 nm). According to the exposure time of 24, 48, and 72 hours Owen´s reagent was added. We also checked the effect of the bortezomib diluent as a vehicle control (VC) and one set of wells were used as a control.

0nm	0.5nm	1nm	2.5nm	5nm	10nm	25nm	50nm	100nm	250nm	VC	control
0nm	0.5nm	1nm	2.5nm	5nm	10nm	25nm	50nm	100nm	250nm	VC	control
0nm	0.5nm	1nm	2.5nm	5nm	10nm	25nm	50nm	100nm	250nm	VC	control
0nm	0.5nm	1nm	2.5nm	5nm	10nm	25nm	50nm	100nm	250nm	VC	control
0nm	0.5nm	1nm	2.5nm	5nm	10nm	25nm	50nm	100nm	250nm	VC	control
0nm	0.5nm	1nm	2.5nm	5nm	10nm	25nm	50nm	100nm	250nm	VC	control
0nm	0.5nm	1nm	2.5nm	5nm	10nm	25nm	50nm	100nm	250nm	VC	control
0nm	0.5nm	1nm	2.5nm	5nm	10nm	25nm	50nm	100nm	250nm	VC	control

Table 3: Scheme of bortezomib treatment, blue: treated with Owen´s reagent, red: non-treated

The treated plates were incubated in the dark at 37°C and a CO_2-atmosphere of 5 % for 2.5 hours. Immediately after that, the color change based on the above descripted reaction was checked with the Spectrostar NANO (BMG LabTech, Ortenberg, Germany) at a wavelength of 490nm. The assay was repeated for three times, so that enough data was produced.

2.5 xCELLigence

To quantify adherent cell proliferation and viability in real time, we used the xCELLigence RD device System for Real-Time and dynamic monitoring of cell proliferation and viability for adherent cells (ACEA Biosciences, Inc., San Diego, CA). The fundamental principle is a non-invasive impedance measurement, according to the decline or increasing number of cells.

For the measurement SW-1353 and primary chondrocytes were seeded in 16-well micro plates (E-plates®, Roche Diagnostics, Rotkreuz, Switzerland). E- Plates are constructed with an undersurface of golden microelectrodes which function as a biosensor for electric current. The electric current is linked to the impedance caused by the number of cells (Figure 9).

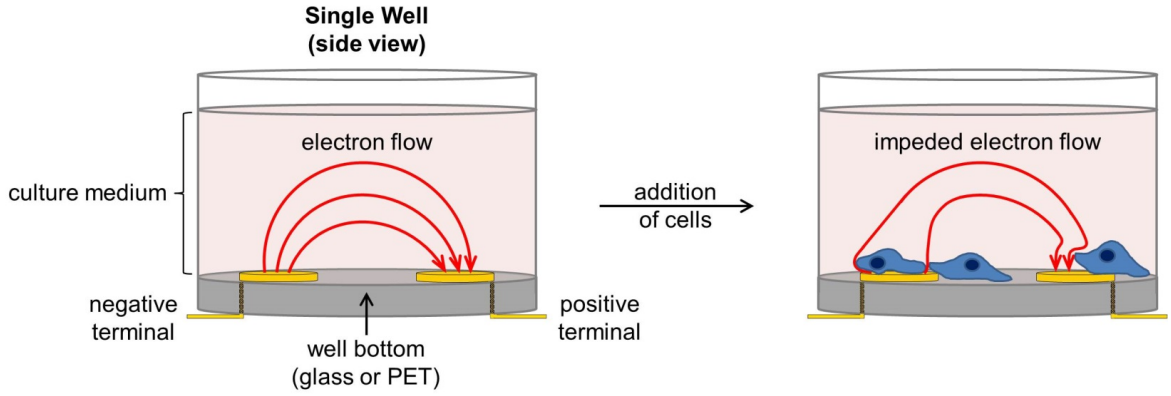

Figure 9: On the left side, the electron flow from the negative to the positive terminal is shown. There are no cells and therefore the impedance is low. On the right, adherent cells were added and block the electron flow. Impedance is high.

(https://www.aceabio.com/wp-content/uploads/xCELLigence-Tech-Overview-Fig-1.jpg)

The curve of impedance versus time is recorded by real time cell analysis software (RTCA 1.2.1. Software; ACEA Biosciences Inc.). However, the impedance is converted into unitless parameter, called Cell Index (CI). This parameter is defined as impedance at time point n minus impedance in absence of cells divided by the nominal impedance value. [34] A theoretical curve is shown in Figure 10.

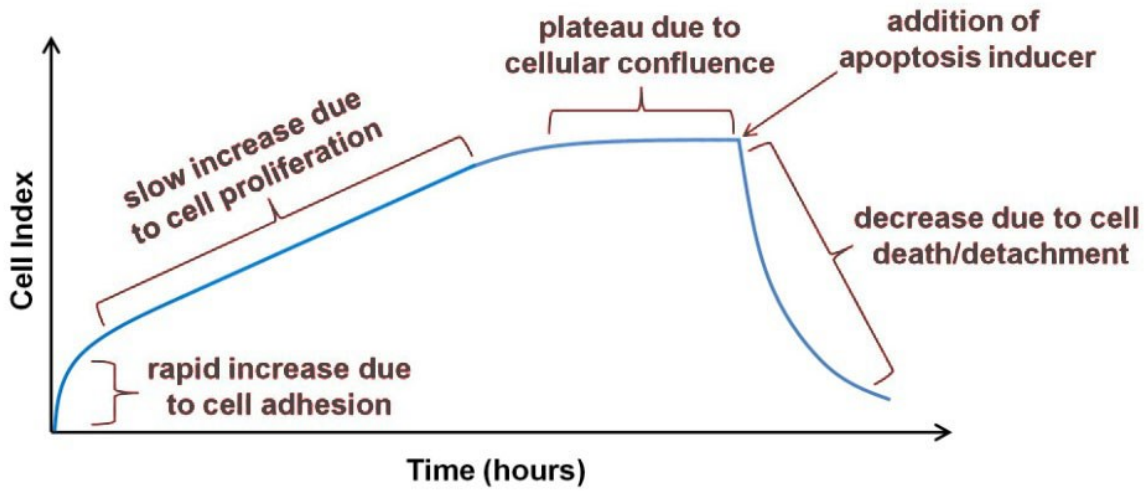

Figure 10: Theoretical curve of xCELLigence. Increasing CI until a plateau due to cellular confluence is reached. By treatment with bortezomib (apoptosis inducer) CI decreases due to cell death/detachment.

(https://www.aceabio.com/wp-content/uploads/xCELLigence-Tech-Overview-Fig-3A.jpg)

2.5.1 Protocol

3000 cells of SW-1353 and primary chondrocytes and 200 µl culture medium were seeded into 16- well E-plates. The E-plates were connected to the RTCA - system and the run was started. On the next day E-plates were disconnected from the system and the culture medium was aspirated. In a next step, the bortezomib treatment with concentrations of 5 nm, 10 nm, and 25 nm and a control were performed. Therefore, we added 100 µl of appropriate concentrations and 100 µl culture medium to the wells. In case of control, we added 200 µl of culture medium. We started the treatment 24 hours later to ensure that the cells form their adherent quality.
In a following step, the connection to the system was recovered again and the run was continued for sixth days. Impedance was measured with the RTCA 1.2.1. Software every 20 minutes. Experiments were repeated three times.

2.6 Fluorescence Activated Cell analysis

We used the BD FACSCalibur™ system (BD Biosciences) to analysis SW-1353 regarding to their specific cell cycle phases under the influence of bortezomib. In a first step, SW-1353 were treated with bortezomib. After treatment, the cells were marked with propidium iodide (PI; Sigma Aldrich, Austria, Vienna). PI is a fluorescence dye that intercalates in the DNA of dead cells and can be used to determine the cell DNA content by fluorescent measurement. [35] Therefore, the amount of discrete PI is directly proportional to the DNA content. According to the DNA content, we can establish a statement about the single cells and their specific cell cycle phases. Because as previously mentioned in the introduction, the DNA content of M-phases is less than DNA-content of S-phases cells.
Before the fluorescent signals are analyzed by software, the BD FACSCalibur™ system separates SW-1353 cells in relation to their size and granularity. In this regard, cells pass a single laser beam that is affected by the specific cell properties. Concerning this matter, we have two important analytical tools, the forward scatter (FSC) and the sideward scatter (SSC) (Figure 11).

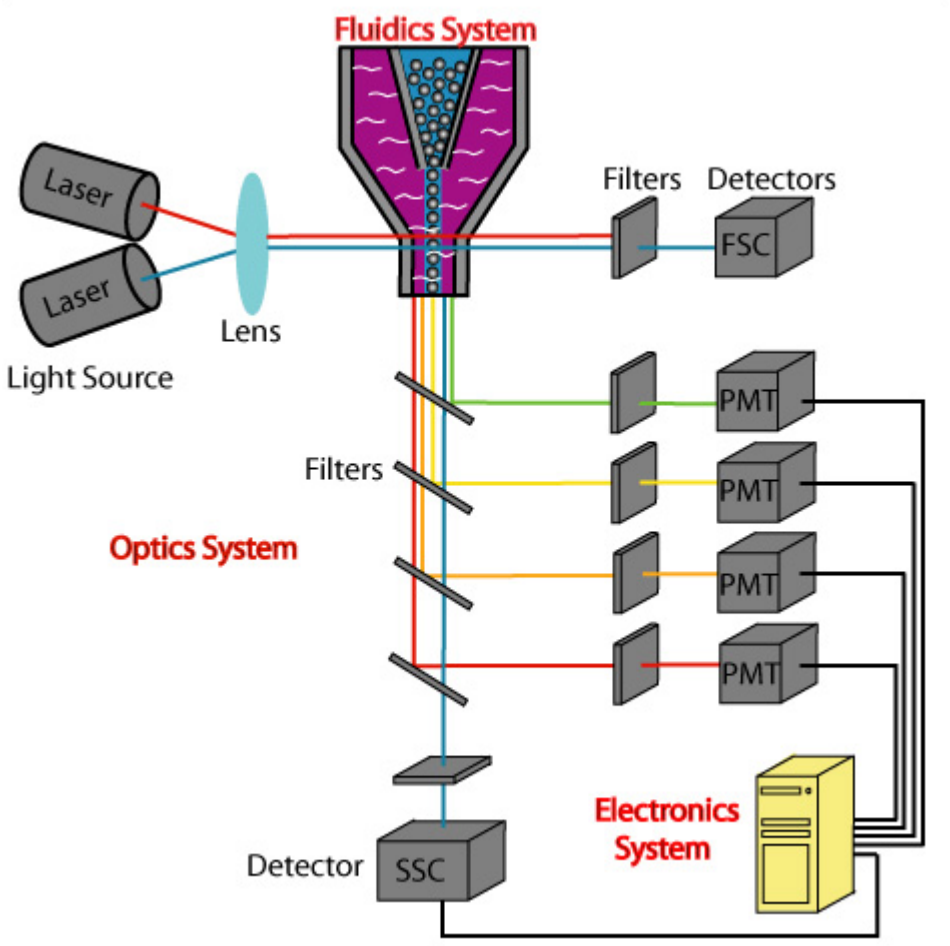

Figure 11: Scheme of flow cytometer

(https://lh5.googleusercontent.com/2d6n-ctpLGz_YiGUm929CagNCxOpfYh14sFBKStfhoFrZwPdadDLpEBfIBljGfRLtvX0yXC7Sbb6Pd-xWBqTYi41rTphpvSVtejAUQAKGIBDcCUk5bBwXaJDExjW9f8x_ruwRWet)

By FSC measurement, cells are discriminated by size due to light diffraction around the cell. The FSC values are detected by a photodiode, which converts light signals into electrical voltage signals, whereby the intensity is proportional to the diameter of the cell. The SSC signal depends on the cell granularity. The granularity influences the refraction of the laser light. When the SSC signal is strong, the granularity is high. [36]

By FSC and SSC signals, the software creates a cloud diagram, which shows a detailed distribution of analyzed cells according to size and granularity (Figure 12).

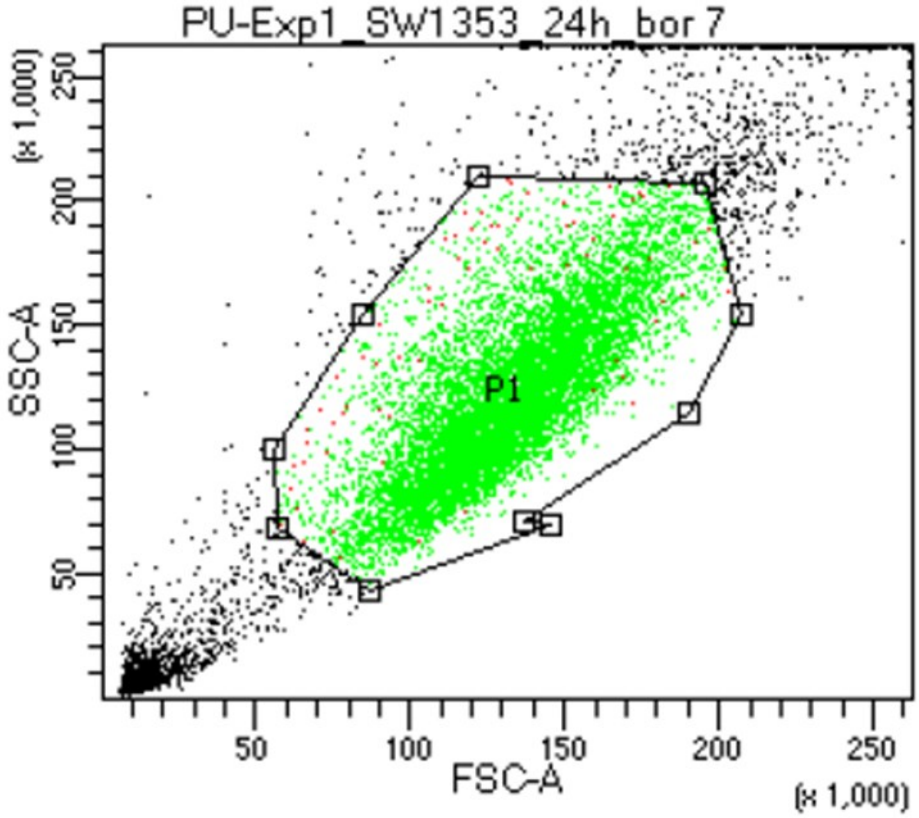

Figure 12: Representative Figure, Cell size and granularity analyzed by FSC and SSC signals. single cells are shown in a cloud diagram, black: debris and doublets, green: cell area used for PI analysis

Based on the cloud diagram a PI analysis is performed. Therefore, it is important to exclude cell doublets (higher values) and debris (lower values) before, because otherwise the measured DNA content would be too high or too low. So, we defined a cell area (green) around 50 to 200 SSC and FSC values for the next analysis step. These around 10000 events of cells are analyzed in terms of PI content (Figure 13).

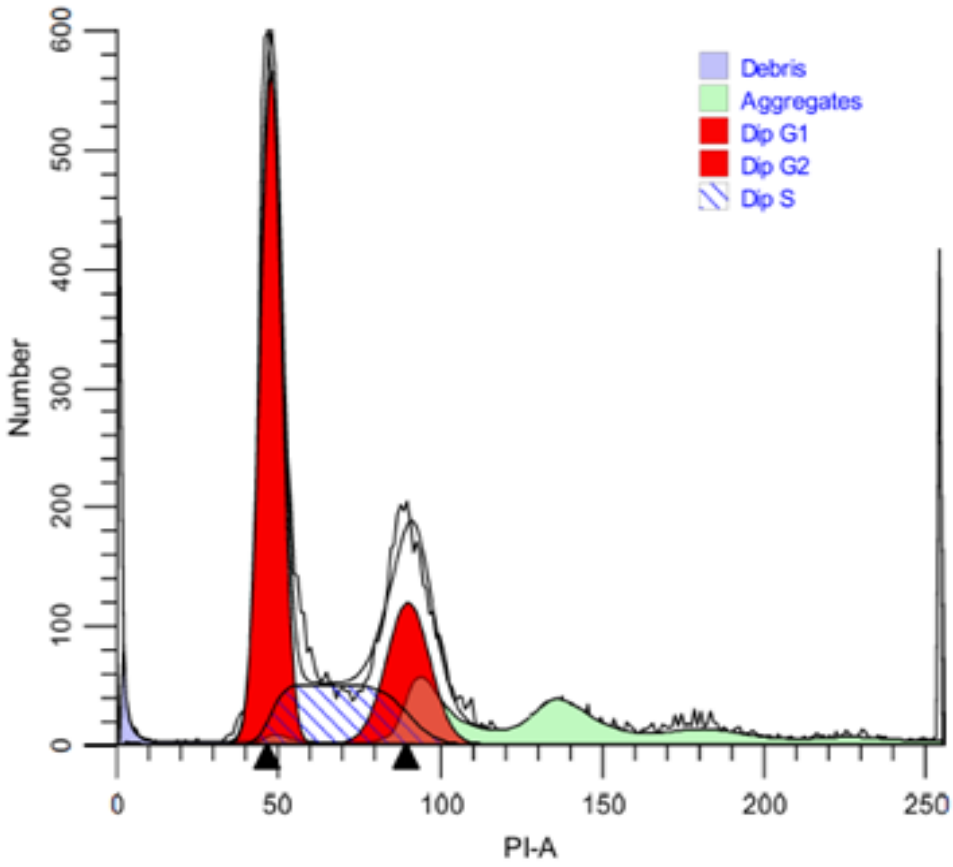

Figure 13: Representative Figure for PI analysis. High PI content reflects G2-Phase, low PI content reflects G1 Phase, in between the S-phase

The percentage distribution of cells concerning the PI content is evaluated statistically and is displayed as a bar chart. Thereby, the PI content is associated with the various phases of the cell cycle.

2.6.1 Protocol

1 x 10^6 SW-1353 with 7 ml of culture medium were seeded into petri dishes. In general, we used three petri dishes (control/ IC25/ IC50) for each timepoint per experiment. We had timepoints of 24 and 48 hours and the experiments were repeated four times. After seeding cells were incubated overnight and next day the treatment was performed. Therefore, we aspirated the culture medium and added 7 ml of the corresponding bortezomib concentrations. Depending on the timepoint, cells were harvested after 24 or 48 hours by Accutase® (Innovative Cell Technologies, San Diego, CA) treatment. The supernatant and the cell suspension was transferred into a 50 ml falcon tube and a centrifugation step with

300 x g for four minutes at 4°C was performed. Now the supernatant was discarded and the cell pellet was resuspended with 5 ml of culture medium. Another centrifugation followed and the supernatant was discarded again. The pellet was resuspended with 0.5 ml of PBS and subsequently the cells were fixed with 5 ml of cold 70% ethanol. These suspensions were stored at a temperature of 4°C until the day of PI staining.
On this day, the cell suspension was centrifugated again with 200 x g for four minutes at 4°C. The cell pellet was solved with hypotonic PI-lysis-buffer (Table 4). Finally, the suspension was transferred into micronics (Micronics, Lelystad, Netherlands) and an incubation of 20 minutes followed. The samples were now ready for analysis by BD FACSCalibur™ system. The samples should be measured within two hours and stored on ice in the dark.

0,1% Natriumcitrat (Sigma, # C-7254)
0,1% Triton X-100 (Fluka, #93418)
100 µg/ml RNAse A (Fermentas, # EN0531)
50 µg/ml PI (Sigma, # P4170)

Table 4: Chemical composition of PI-lysis-buffer

To produce hypotonic-lysis-buffer we had to make some dilutions. 1 g of Natriumcitrat was solved with 10 ml distilled water. We did the same with 1ml of Triton X-100. In case of RNAase, we used a stock solution (10mg/ml). 25 mg of PI was solved in 25 ml of PBS. These dilutions were used to produce 50 ml of hypotonic PI-lysis-buffer. So, we added 0.5 ml of 10% Natriumcitrat, 0.5 ml of 10% Triton-X-100, 0.5 ml RNAase A and 2.5 ml PI to 46 ml destilled water.

2.7 Real – time quantitative Polymerase Chain Reaction

Since the invention of the Polymerase Chain Reaction (PCR) by Kary Mullis at Cetus Corporation in 1985 the course of molecular science changed rapidly. [37] Today the method of PCR is used on many ways. For example, in the examination of nucleotide sequence variations [38-40] and chromosomal rearrangements [41], for high-efficiency

cloning of genomic sequences [42], for direct sequencing of genomic DNAs [43,44] and for the detection of viral pathogens. [45]

PCR is an effective amplification method that enables us to generate large quantities of specific DNA segments based on a small amount of starting material. The PCR requirements are DNA template, primers, nucleotides and the most important enzyme, DNA polymerase. This enzyme links single nucleotides from the 3´-end to the 5´- end to form the PCR product. To amplify a specific region, the use of primers is necessary. Primers are small DNA fragments with a defined sequence binding to a complementary region of the target DNA. They function as a starting point for DNA-Polymerase.

This mixture is given to a test tube and placed in a PCR- machine. After that, three major steps follow. In a first step, the denaturation of the DNA template is performed by heating above the melting point of the two complementary DNA strands. In a next step, the temperature is reduced to allow the annealing of specific primers to the target DNA segment. In a last step, the temperature is raised again to create optimal conditions for the DNA- Polymerase. After all, a small DNA fragment is amplified. In general, these steps can be repeated a thousand of times, so that the DNA content raises explosive. [46]

A schematic overview of PCR is shown in Figure 14.

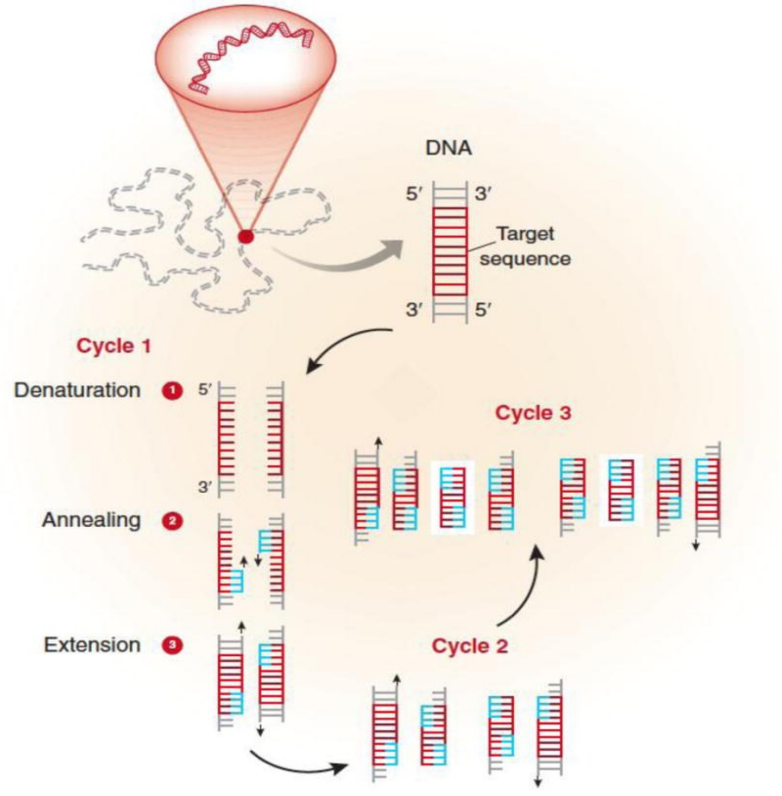

Figure 14: Schematic overview of PCR

(https://www.ncbi.nlm.nih.gov/pmc/articles/PMC4102308/bin/nihms593299f1.jpg)

In earlier times, the quantification of amplified PCR products was performed after the PCR reaction via time-consuming gel electrophoresis and image analysis. Nowadays the Real-time quantitative PCR (qRT-PCR) makes it possible to amplify and to quantify in one step. Therefore, a fluorescent dye is additionally needed. The used fluorescent dyes can bind to double-stranded DNA, are molecules attached to PCR primers or probes that hybridize with PCR product during amplification. As a result, a qRT-PCR device can quantify the produced PCR products with increasing fluorescent signals after every cycle and therefore, it is also possible to differentiate between early and late expressed genes. The earlier the fluorescent signal appears, the bigger was the content of gene product. [47]

In this study qRT-PCR was used to analysis the change of CDK1, CDK2, cdc25, CCNB, CCNA gene expression after IC25 and IC50 treatment of bortezomib.

Before the qRT-PCR protocol is mentioned, we must emphasize some preparatory work, like RNA isolation and analysis, removal of genomic DNA and complementary DNA (cDNA) synthesis.

2.7.1 RNA – Isolation

We used the RNeasy Mini Kit (Qiagen) to purify the RNA. In this progress, the RNA was bound by means of microspin technologies speed by a silica-based membrane. For this purpose, SW1353 and primary chondrocytes samples had to be lysed in a first step to release the whole RNA content. In a next step, the lysate was homogenized and denatured by a guanidine – thiocyanate containing buffer. This buffer inactivated RNAses whereby the purification of intact RNA was ensured. In the following step, Ethanol was added for optimal binding conditions. After all, the sample was transferred to an RNeasy Mini spin column. Therefore, disruptive factors for PCR, like genomic DNA, cell debris, proteins and other substances were eliminated and the RNA was bound to the membrane by using a specific high-salt buffer system. High-quality RNA could now be eluted by 30-100 µl water [48] (Figure 15).

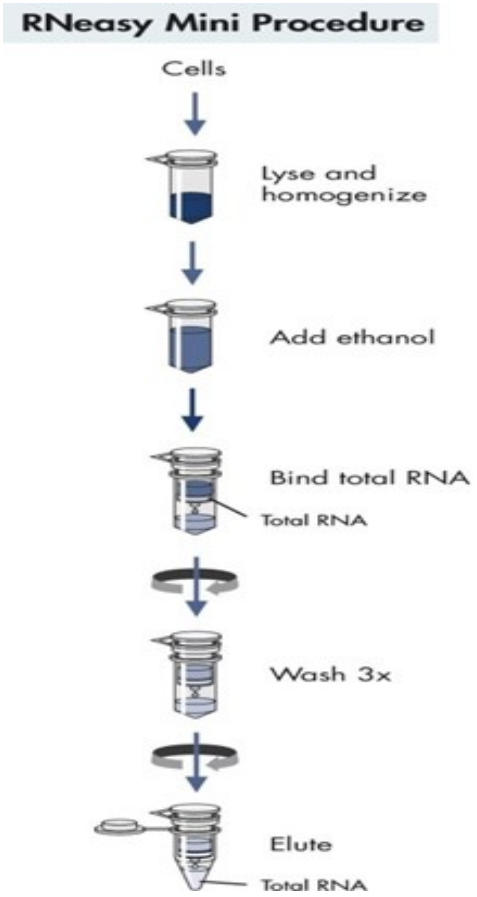

Figure 15: Schematic overview of RNeasy Mini procedure

(https://www.qiagen.com/~/media/nextq/image%20library/fc/01/71/fc_0171_rneasymini/1_8.ashx)

2.7.1.1 Protocol

2 x 10^6-cells of SW-1353 with 7 ml of culture medium were plated into petri dishes. Three dishes were used for control, IC25- and IC50-treatment. The treatment was performed 24 hours after seeding and RNA was isolated after 48 hours of exposure time. In general, samples were produced in quadruplicates.

To start the experiment, we had to do some preparatory work. 10 µl β-mercaptoethanol per 1.0 ml RLT buffer (Qiagen) was added and a solution of 70% ethanol was produced. We washed the cells with 37°C PBS 1x and subsequently, we started lysing by pipetting 175 µl modified RLT buffer into each of the petri dishes and harvested our cells by using a cell scraper. Detached cells were transferred into spin columns. Spin columns have been prefilled with 350 µl of 70 % ethanol before. The spin columns were centrifugated at 10.000 rpm for 30 seconds and the flow-through was discarded.

Three other steps followed. At first, 700µl RW1 buffer was added. In a next step, 500 µl RPE was added and repeated for a second time. Every step was accompanied by another centrifugation at 10.000 rpm for 30 seconds and the flow-through was discarded again.
For best results, the collection tubes were renewed and the membrane of the spin-columns were dried by spinning at 10.000 rpm for 1 minute. RNA was isolated and diluted with 30 µl of RNase-free water by a last spinning task at 10.000 rpm for 1 minute.
To check the concentration and the purity of the isolated RNA we used the NanoDrop system (eqLab Biotechnologie GmbH, Erlangen, German). Thereby, the optical density (OD) was photometrically measured at wavelengths of 260 nm (absorption maxima of nucleic acids) and 280 nm (absorption maxima of proteins). For the determination of the RNA purity, the ratio between OD_{260} and OD_{280} was defined whereby a ratio higher than 1.8 is acceptable for gene expression measurements. [49,50] After all RNA samples were stored at -70°C.

2.7.2 Bioanalyzer

In addition to NanoDrop technology, we used the Agilent 2100 BioAnalyzer (Agilent Technologies, Santa Clara, CA) for quality control of purified RNA. The Agilent 2100 Bioanalyzer (Agilent Technologies) combines the technique of capillary electrophoresis with a fluorescent dye measurement for defining the total RNA concentration and integrity. This lab-on-chip system consists of sample wells, gel wells and a well for an external standard (ladder), which are all connected by glass micro-channels to create an interconnected network.
For chip preparation, the micro-channels were filled with a sieving polymer and a fluorescence dye that could bind to RNA. Then, in case of using Nano Chip kit, twelve samples and ladder with marker was loaded in each well.
The loaded chip was connected to an electrical circuit, so that RNA was electrophoretically ripped by a voltage gradient. Charged RNA was separated by size whereby smaller fragments moved faster than larger ones. During the migration, fluorescent dye intercalated into RNA strands and therefore RNA could be measured by fluorescent detection. Sample data was translated into gel-like images and electropherograms and compared with the RNA 6000 ladder standard.
For a better reproducibility, Agilent company introduced the RNA Integrity Number (RIN) based on a software algorithm including all electrophoretic traces. This unitless scale

ranges from 1 to 10 whereby 1 is for the most degraded RNA and 10 for the most intact RNA. For RT-PCR RINs higher than 5 might work, optimal RINs should be higher than 7/8.
In general, the study was performed according to the Agilent RNA 6000 Nano Kit Guide protocol. [51]

2.7.3 Removal of genomic DNA

To get DNA-free RNA for PCR, we used the Thermo Scientific™ DNase I, RNase-free kit (Thermo Fisher Scientific).
This kit is based on the endonuclease DNAase I, which fragmentizes, single- and double stranded DNA by hydrolyzing phosphodiester bonds. Including the kit, a buffer with magnesium-chloride ($MgCl_2$) is added. The 10x reaction buffer itself consists of 100 mM Tris-HCl (pH 7.5 at 25°C), 25 mM $MgCl_2$ and 1 mM $CaCl_2$. Therefore, the Mg^{2+}-ions are indispensable for the enzyme activity. [52]

2.7.3.1 Protocol

We added 1 µg (maximum volume 8 µl) of isolated RNA to 1 µl 10x reaction buffer and 1 µl DNAse I, RNase-free. Diethylpyrocarbonate-treated water was used to fill up until a total volume of 10 µl.
Afterwards the mixture was incubated at 37°C for 30 minutes to start the enzymatic degradation. We inactivated the enzyme by adding 1 µl of 50 mM ethylenediaminetetraacetic-acid (EDTA) and attached another incubation at 65°C for 10 minutes.

2.7.4 Complementary DNA Synthesis

iSCript cDNA Synthesis Kit (Biorad, Hercules, CA) was applied to synthesis complementary DNA (cDNA). The iScript cDNA synthesis kit is a very sensitive tool for first-strand cDNA synthesis according to gene expression analysis using real-time qPCR. The kit´s core is a modified Moloney Murine Leukema Virus-derived reverse transcriptase enzyme which connects oligonucleotides starting from a specific primer molecule.

Oligonucleotides and primers are provided by a 5x iScript reaction mix, the second tube of cDNA Synthesis Kit. [53]

2.7.4.1 Protocol

To create the reaction mixture, we added 11 µl RNA to 4 µl of 5x iScript reaction mix and 1 µl of iScript reverse transcriptase. In a following step, 4 µl of nuclease-free water was added to a total volume of 20 µl. The reaction itself was performed according to Table 5.

Time (minutes)	Temperature (°C)
5	25
30	42
5	85
Hold	4

Table 5: Reaction protocol of cDNA synthesis

2.7.5 RT-qPCR

The SsoAdavanced™ Universal SYBR® Green Supermix (BioRad) was used to perform the RT-qPCR reaction with a CFX96 Touch Real-Time PCR Detection System (BioRad). The supermix contains buffer, dNTPs, thermostable hot-start DNA polymerase and SYBR Green dye. [54]

SYBR Green is an intercalating fluorescent dye that directly binds between the DNA bases of double stranded DNA. By detecting the fluorescence during each amplification cycle of PCR, it is possible to quantify the amplified DNA. [55]

Additional to 5 µl of SYBR Green supermix, 1 µl of quantitect Primer 10x, 3 µl of nuclease free water and 1 µl of the RNA template were pipetted to the PCR plate. For the examination of the target genes and reference genes, all used primers (Table 6) and PCR substances were pipetted in triplicates according to the pipetting scheme as shown in Table 7.

Reference Gene QuantiTect® primer assays (Qiagen, Hilden, Germany)	**Abbreviation**	**Catalogue number**
β-Actin	ACTB	QT00095431
Hypoxanthine phosphoribosyl-transferase	HPRT	QT00059066
Target Gene QuantiTect® primer assays (Qiagen, Hilden, Germany)	**Abbreviation**	**Catalogue number**
Cyclin A	CCNA	QT00052941
Cyclin B	CCNB	QT00006615
Cyclin-dependent-kinases 1	CDK1	QT00042672
Cyclin-dependent-kinases 2	CDK2	QT00005586
Cell-division-cycle 25	Cdc25	QT00000350

Table 6: QuantiTect® primer assays

1	1	2	3	4	5	6	7	8	9	10	11	12
A	ACTB SW1353 KO	ACTB SW1353 KO	ACTB SW1353 KO	ACTB SW1353 5nM	ACTB SW1353 5nM	ACTB SW1353 5nM	ACTB SW1353 10nM	ACTB SW1353 10nM	ACTB SW1353 10nM	ACTB NTC	ACTB NTC	ACTB NTC
B	HPRT SW1353 KO	HPRT SW1353 KO	HPRT SW1353 KO	HPRT SW1353 5nM	HPRT SW1353 5nM	HPRT SW1353 5nM	HPRT SW1353 10nM	HPRT SW1353 10nM	HPRT SW1353 10nM	HPRT NTC	HPRT NTC	HPRT NTC
C	CCNA SW1353 KO	CCNA SW1353 KO	CCNA SW1353 KO	CCNA SW1353 5nM	CCNA SW1353 5nM	CCNA SW1353 5nM	CCNA SW1353 10nM	CCNA SW1353 10nM	CCNA SW1353 10nM	CCNA NTC	CCNA NTC	CCNA NTC
D	CCNB SW1353 KO	CCNB SW1353 KO	CCNB SW1353 KO	CCNB SW1353 5nM	CCNB SW1353 5nM	CCNB SW1353 5nM	CCNB SW1353 10nM	CCNB SW1353 10nM	CCNB SW1353 10nM	CCNB NTC	CCNB NTC	CCNB NTC
E	CDK1 SW1353 KO	CDK1 SW1353 KO	CDK1 SW1353 KO	CDK1 SW1353 5nM	CDK1 SW1353 5nM	CDK1 SW1353 5nM	CDK1 SW1353 10nM	CDK1 SW1353 10nM	CDK1 SW1353 10nM	CDK1 NTC	CDK1 NTC	CDK1 NTC
F	CDK2 SW1353 KO	CDK2 SW1353 KO	CDK2 SW1353 KO	CDK2 SW1353 5nM	CDK2 SW1353 5nM	CDK2 SW1353 5nM	CDK2 SW1353 10nM	CDK2 SW1353 10nM	CDK2 SW1353 10nM	CDK2 NTC	CDK2 NTC	CDK2 NTC
G	Cdc25c SW1353 KO	Cdc25c SW1353 KO	Cdc25c SW1353 KO	Cdc25c SW1353 5nM	Cdc25c SW1353 5nM	Cdc25c SW1353 5nM	Cdc25c SW1353 10nM	Cdc25c SW1353 10nM	Cdc25c SW1353 10nM	Cdc25c NTC	Cdc25c NTC	Cdc25c NTC
H	x	x	x	x	x	x	HPRT RT-	HPRT RT-	HPRT RT-	HPRT NK	HPRT NK	HPRT NK

Table 7: Pipetting scheme for PCR: Primers are applied as triplicates (KO = control, NTC = Non-target control, NK = negative control, RT- = without Reverse Transcriptase)

In the following step, the plate was vortexed for optimal mixing of all ingredients and centrifugated at 900 rounds per minute (rpm) for 1 minute. After that, the plate was ready for the run and loaded to the CFX96 Touch Real-Time PCR Detection System (BioRad). The setting of the PCR run is shown in Figure 16.

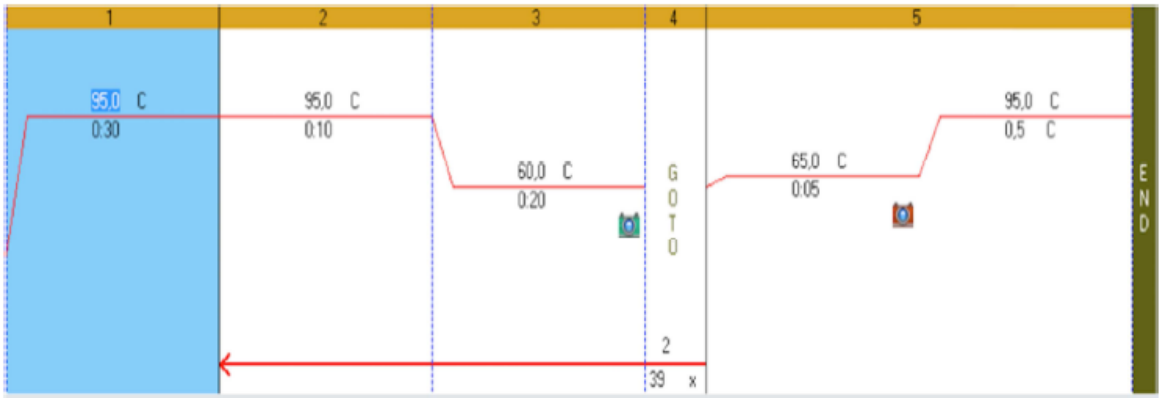

Figure 16: Thermo-cyclic-repeated protocol of PCR

In a first step, the DNA denaturation and polymerase activation took place at 95°C for 30 seconds. Another denaturation step was connected at 95°C for 10 seconds. In the following step, the annealing was performed at 60°C for 20 seconds and the plate was read. The PCR cycle up to here was repeated for 39 times and in a last step a melt curve analysis at 65°C for 5 seconds to 95°C for 50 seconds was performed to define the specificity of the amplification (Figure 17). Furthermore, the plate was read again.

Following the RT-PCR analysis, the expression level (C_t) of the target gene was normalized to the reference genes (ACTB, HPRT-1) (ΔC_t) and then the ΔC_t of the test sample was normalized to the ΔC_t of the controls ($\Delta\Delta C_t$). Finally, the expression ratio was calculated with the $2^{-\Delta\Delta Ct}$ method ($*p < 0.05$). [56]

2.8 Statistical analysis

All data were expressed as mean ± SD. A Student's unpaired t-test was executed to show significant differences between bortezomib treated cells and control cells. For adequate data material, all experiments were repeated up to four times. Graphic analyses were performed by Sigma Plot® (Systat Software Inc., San Jose, CA) or Microsoft Excel 2010 (Microsoft, Washington, WA).

3 Results

3.1 Vimentin – DAPI Immunofluorescence

Vimentin – DAPI Immunofluorescence was performed to specify the origin of primary chondrocytes and SW-1353 by means of vimentin structures. As a mesenchymal structure, vimentin could be documented by labeled antibody-antigen interactions. Therefore, a high content of green fluorescence recorded the mesenchymal origin of primary chondrocytes and SW-1353. The monoclonal anti-vimentin antibody bound to the cytoskeletal structure of vimentin. These bindings were revealed by a second cyanin-2 conjugated goat anti-mouse antibody shown in Figure 17 (a-c) and Figure 18 (a-c).

We also checked the fluorescence behavior of primary chondrocytes and SW-1353 under the influence of AB-diluent and unspecific IgG antibodies. Therefore, no green fluorescence appeared. The cy-2 conjugated goat anti-mouse antibody was not able to bind any structures.

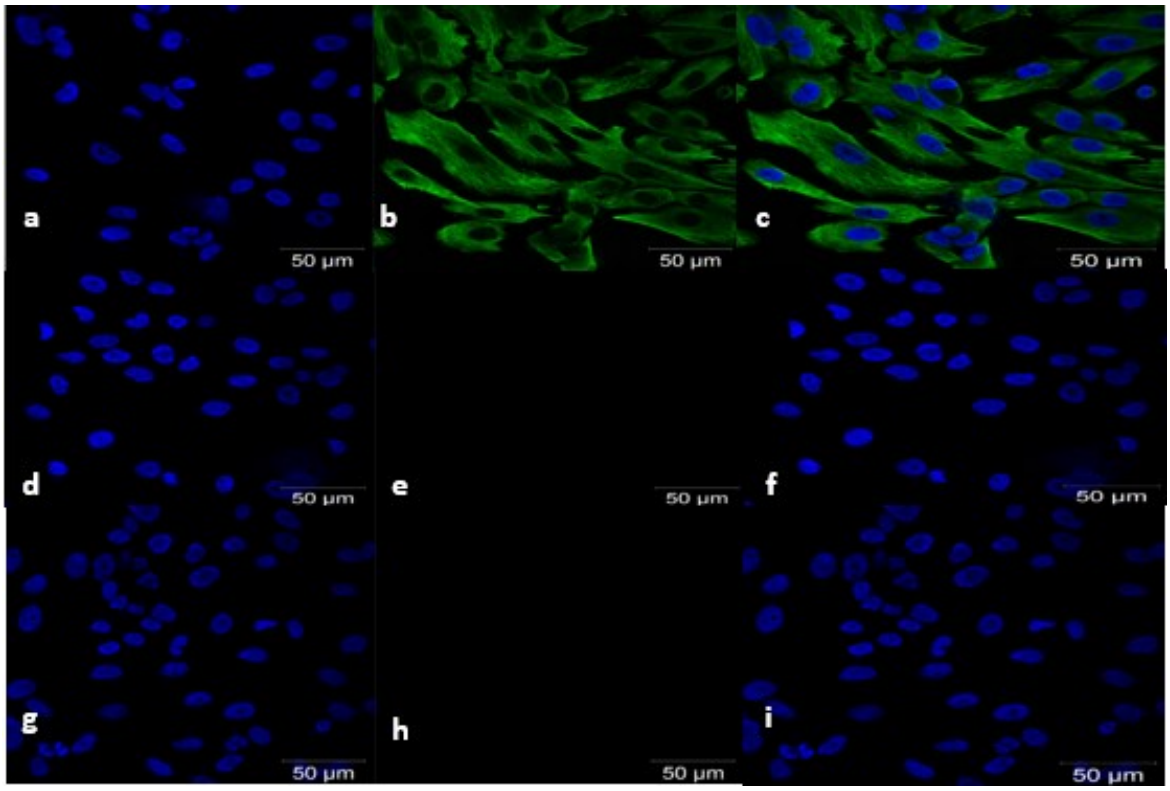

Figure 17: Primary chondrocytes fluorescence Images.

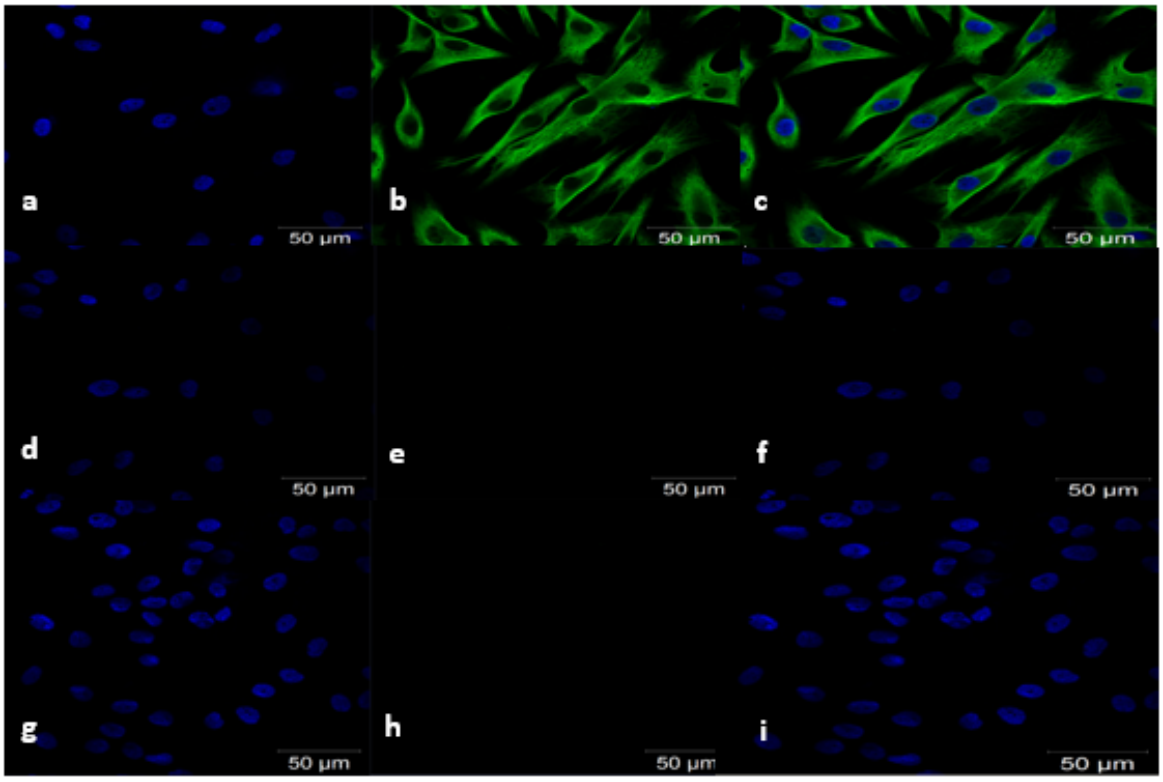

Figure 18: SW-1353 fluorescence Images.

3.2 STR- Analysis

We performed STR- Analysis of SW-1353 to have a genetic evidence for the compliance of the same origin of our used cells and recorded SW-1353 cells in the German Collection of Microorganism and Cell Cultures (DMSZ) database. Therefore STR-Loci were compared. By a compliance of eight or more STR-loci, the evidence is done.

In our case, we had agreements in the following nine STR- Loci: TH01, D5S818, D13S317, D7S820, D16S539, CSF1PO, Amelogenin, vWA, and TPOX (Table 8).

STR-Locus	your cell line	DSMZ
D3S1358	15,18	
TH01	6,9	6,9
D21S11	30, 32.2	
D18S51	13,17	
Penta E	12,14	
D5S818	10,11	10,11
D13S317	12,13	12,13
D7S820	9,11	9,11
D16S539	11,12	11,12
CSF1PO	12	12
Penta D	10,11	
Amelogenin	X	X
vWA	16,17	16,17
D8S1179	10,11	
TPOX	8,11	8,11
FGA	22,23	

Kit: Promega, PowerPlex 16HS System (Cat.No. DC2101)

Table 8: Agreements of STR-Loci, SW-1353 was compared to DMSZ database cells

3.3 Cell viability assay

The CellTiter 96 AQueous One Solution Cell Proliferation Assay (Promega) was performed to evaluate the effects of bortezomib to the viability of primary chondrocytes (C15/C23) and SW-1353. Cells were treated with concentrations of 0 nm, 0.5 nm, 1 nm, 2.5 nm, 5 nm, 10 nm, 25 nm, 50 nm, 100 nm, and 250 nm. Effects were proved by a colorimetric method at a wavelength of 490 nm about the Owen´s reagent reaction after 24, 48 and 72 h. All experiments were performed in quadruplicates and all values are presented as means ± standard deviation.

According to C15/C23 could be seen, that there were no viability changes for the exposure time of 24 h. Unreliable of the raise in concentration, the viability remained approximately to 100 %. After 48 h, the viability fell off to the value of 58 %. The decrease could be

recorded at a concentration of 2.5 nm. At timepoint 72 h, the decrease was more pronounced. Viability fell off up to 70 % with increasing concentrations (Figure 19).

According to SW-1353 could be seen, that the viability already changed after a treatment of 24 h. A linear decrease up to 60 % could be registered with increasing concentrations. We had statistical outliers at a concentration of 10 nm. Therefore, pipetting problems might be the reason. For 48 and 72 h, the optical density (OD) values were too high at the beginning, because of too many cells per well. So, the effects of 0.5 nm and 1 nm were difficult to evaluate, but at a concentration of 2.5 nm a decrease was detectable for both timepoints. After 48 h, the decrease was up to 70 % and after 72 h even up to 100 % (Figure 19).

In general, we could also state that concentrations between 2.5 nm and 25 nm had the greatest influence on primary chondrocytes and SW-1353 (Figure 19).

In relation to the single timelines, a comparison between C15/23 and SW1353 showed that bortezomib influenced the tumor cells more than healthy chondrocytes unreliable of the exposure time (Figure 20).

Furthermore, we defined the half maximal inhibitory concentration (IC50) of bortezomib by means of the CellTiter 96 AQueous One Solution Cell Proliferation Assay. This value was 7.5 nm and was used for the following experiments.

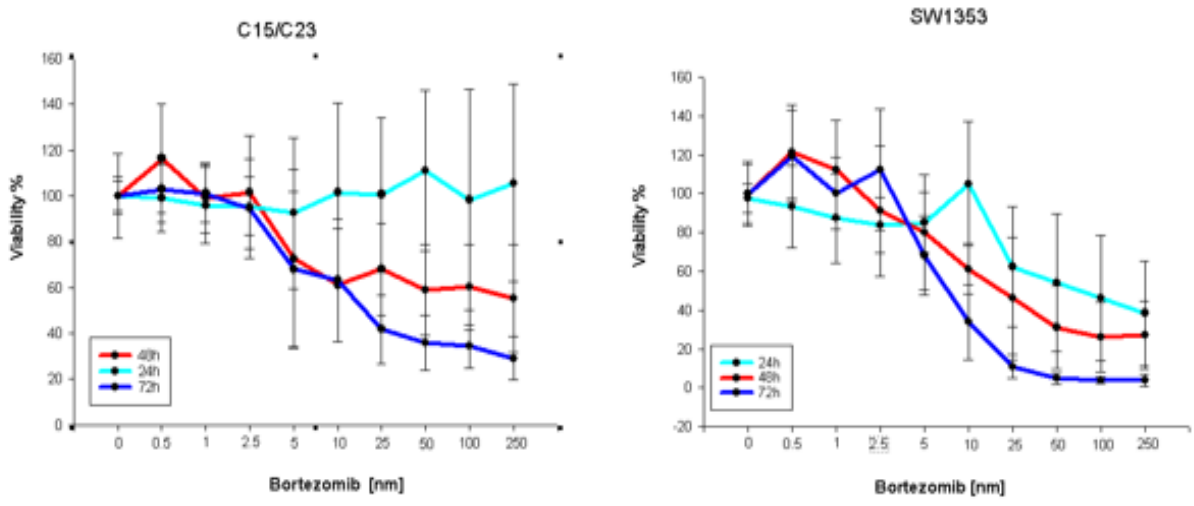

Figure 19: Viability behavior of C15/23 and SW-1353 under the influence of increasing concentrations of bortezomib for the exposure times of 24, 48 and 72 hours.

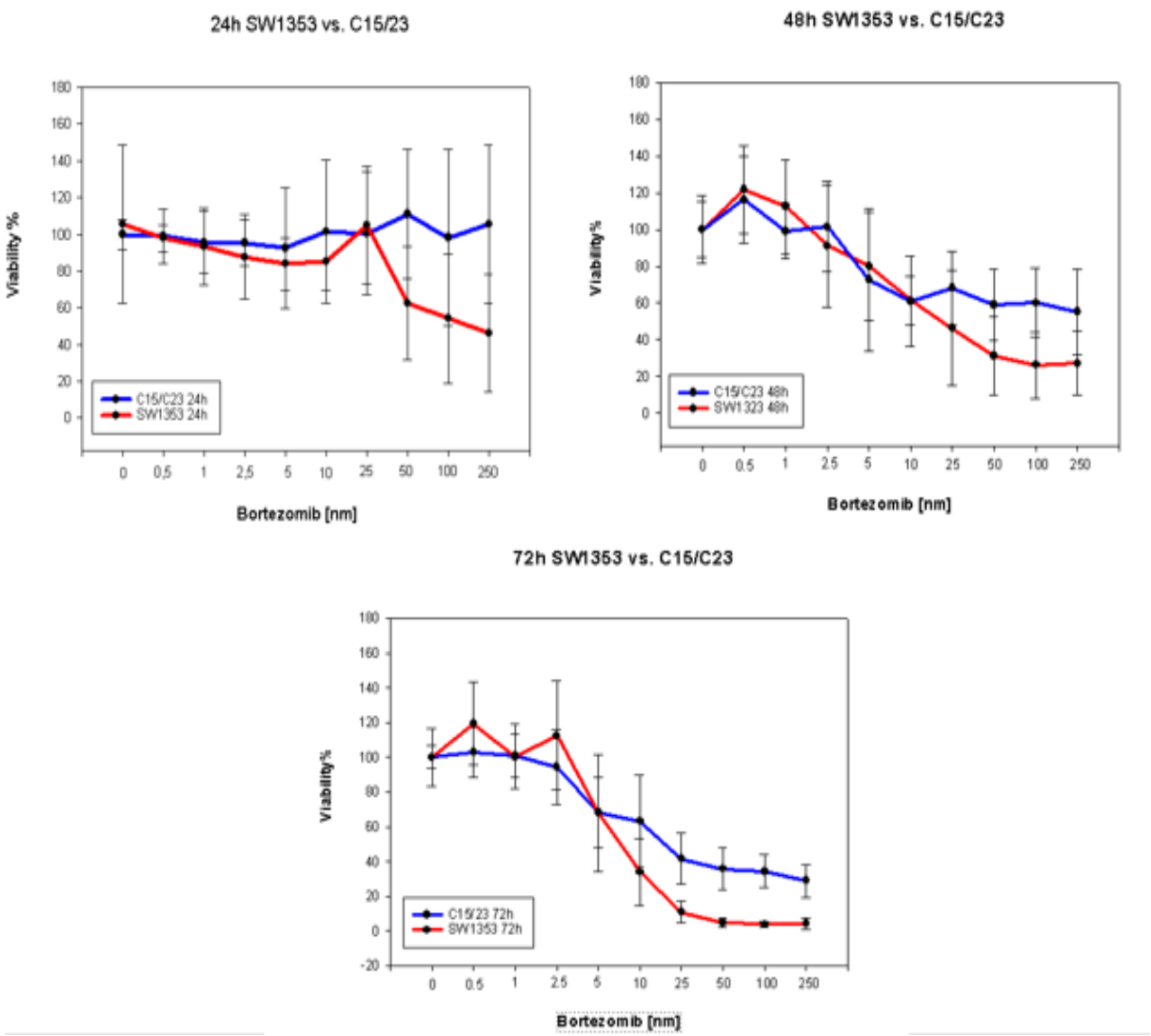

Figure 20: Comparison between single timelines of treated C15/23 and SW1353

3.4 xCELLigence

The Influence of Bortezomib to the cell proliferation in real-time was checked by the xCelligence system. Therefore, 3000 cells of primary chondrocytes and SW-1353 were seeded into each well of a 16-well-plate and were treated with bortezomib concentrations of 0 nm, 5 nm, 10 nm, and 25 nm. In accordance with the functional principle of the xCELLigence, the cell index was measured every 20 minutes for five days by RTCA 1.2.1 Software. All experiments were performed in triplicates and all values are presented as means ± standard deviation.

In response to the curves of primary chondrocytes, the control curve showed a continuous growth until a plateaued peak at around CI 1.5. This course complied with the theoretical

curve of Figure 10. With a 5 nm treatment, the proliferation seemed to be in a delayed manner. Nevertheless, the CI began to raise after an observation period of 80 h. Within the scope of 120 h the CI was around 0.75 at the end. However, it could not be ruled out that values like the control could be reached by longer observation times. For the treatments of 10 nm and 25 nm, the values were close to zero. No proliferation appeared within 120 h, but also here an increase of CI could be possible after more than five days (Figure 21).

SW-1353 cells showed a very similar pattern in the observation time. The control curve increased linear up to CI values of ≥ 6 within 120 h. At this point, it should be stated, that the CI not only depends on the increasing number of cells, but also on cell morphology and size. Therefore, tumor cells were predominant and the CI was correspondingly higher.

For the curve of 5 nm bortezomib, the proliferation was delayed again, but interestingly shorter. The cells already started growing after 60 h. CI raised up to 4.2 within 120 h. This concluded, that bortezomib of low concentration effected tumor cells less than primary chondrocytes. Plateau levels were not obvious in case of control and 5 nm treatment. No proliferation was registered by higher concentrations. The CI for 10 nm was continuously around 1 and the CI for 25 nm was close to zero. Even here, proliferation could be possible after more than 120 h (Figure 22).

These data in combination with the results of the viability assay show a dose- and time-depending influence of bortezomib to the cell proliferation. Apart from 5 nm treatment, cell death increases with higher concentrations and time.

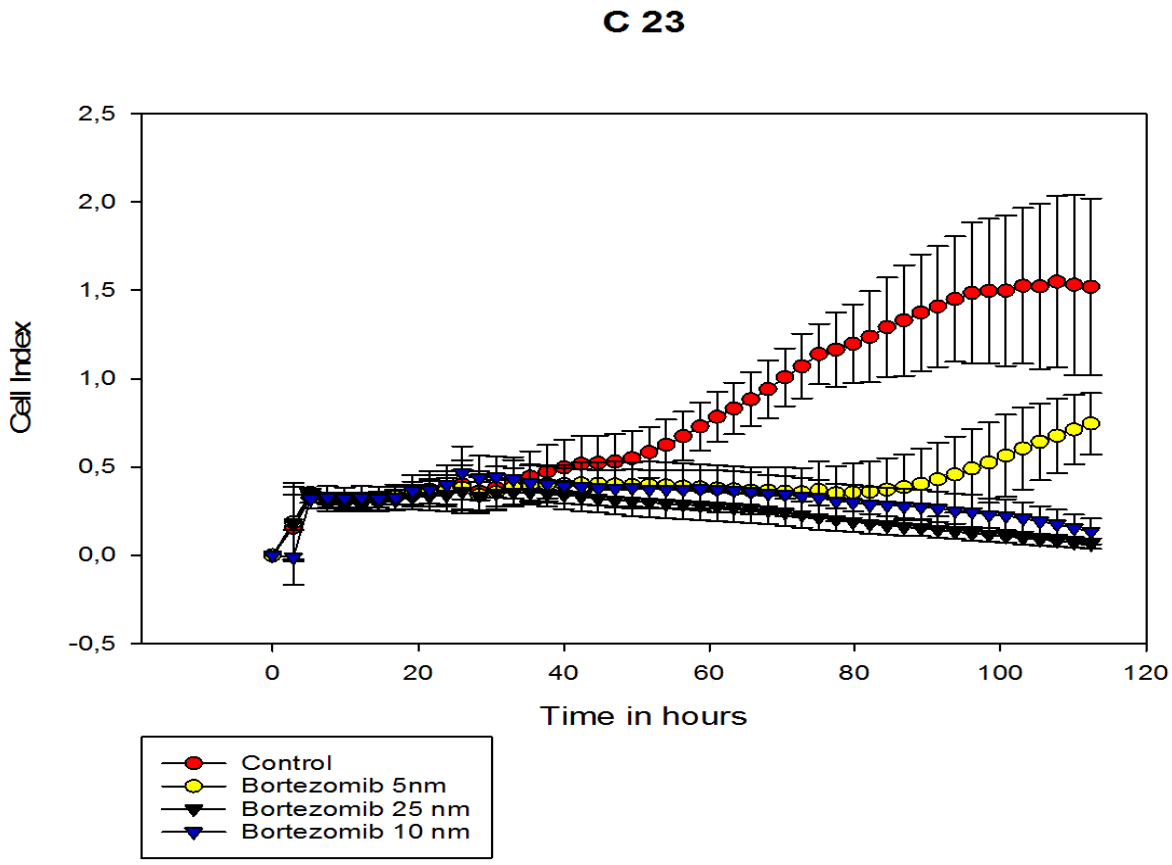

Figure 21: Primary chondrocytes -- xCELLigence

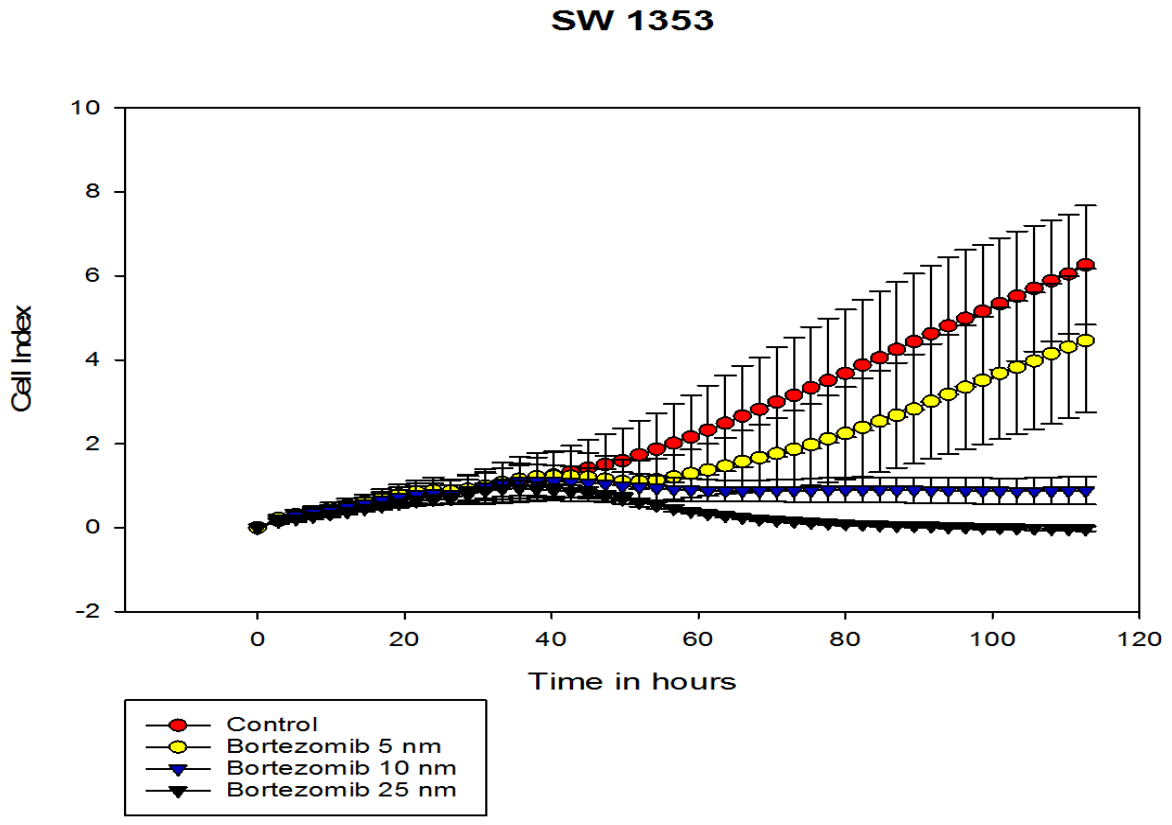

Figure 22 : SW-1353 -- xCELLigence

3.5 Cell cycle FACS analysis

The influence of bortezomib to the cell cycle distribution was investigated by the BD FACSCalibur™ system. In this progress, tumor cells were treated with concentrations of 3.75 nm (IC25) and 7.5 nm (IC50) for 24 and 48 h. Every sample was produced in quadruplicates and was compared to control groups. The change in the percentage distribution of the single cell cycle phases was analyzed and the mean for G1, G2 and S phase was calculated. The results were presented by bar charts according to the IC25 and IC50 treatment.

For the exposure time of 24 hours and IC25 treatment, we could verify a significant ($p < 0.05$) decrease of S-phase cells. G1 and G2 phase cells seemed to be increased, but no significance ($p > 0.05$) was detectable. In higher concentration (IC50), bortezomib effected significant changes in all cell cycle phases. We had a reduction of S- ($p < 0.01$) and G1-phase ($p < 0.05$) cells and a highly significant increase of G2 phase ($p < 0.001$) (Figure 23).

For the exposure time of 48 hours, we could only verify a significant increase of G2 – phase ($p < 0.01$) cells after an IC50 treatment. No significant changes appeared for S- and G1 phase. According to the IC25 treatment, significance was not detectable at all (Figure 23).

Referring to these results, bortezomib seems to be mainly effective at the G2/M checkpoint.

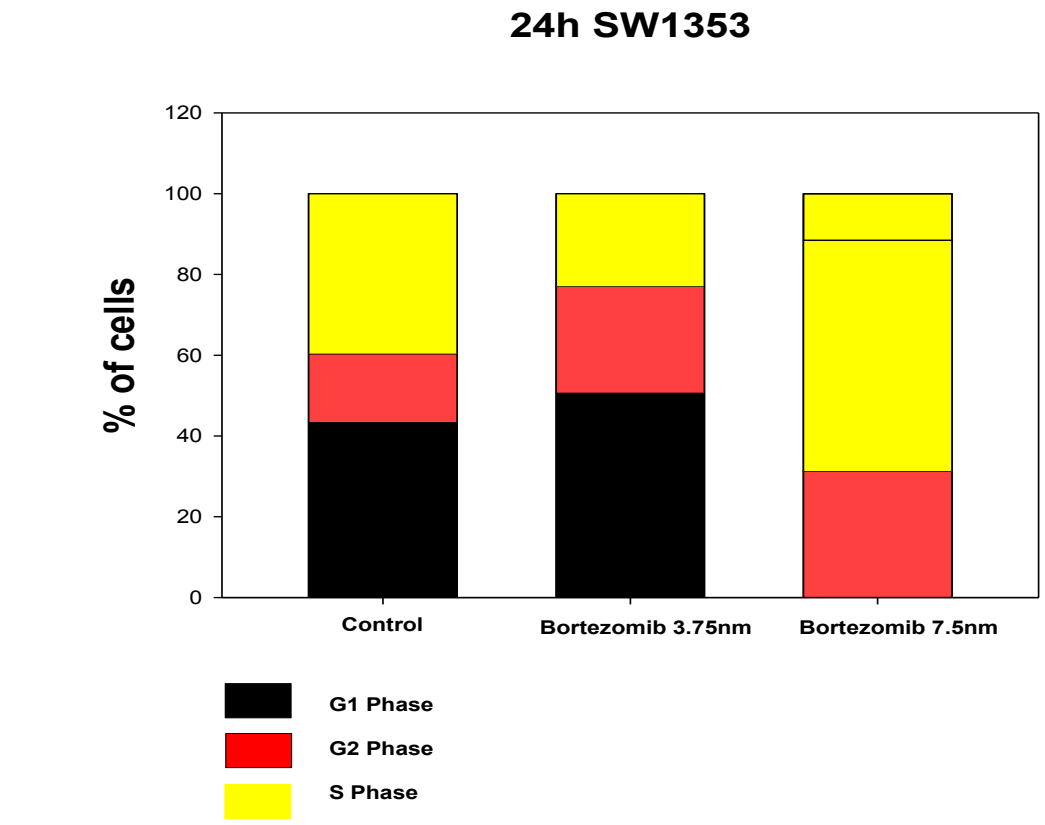

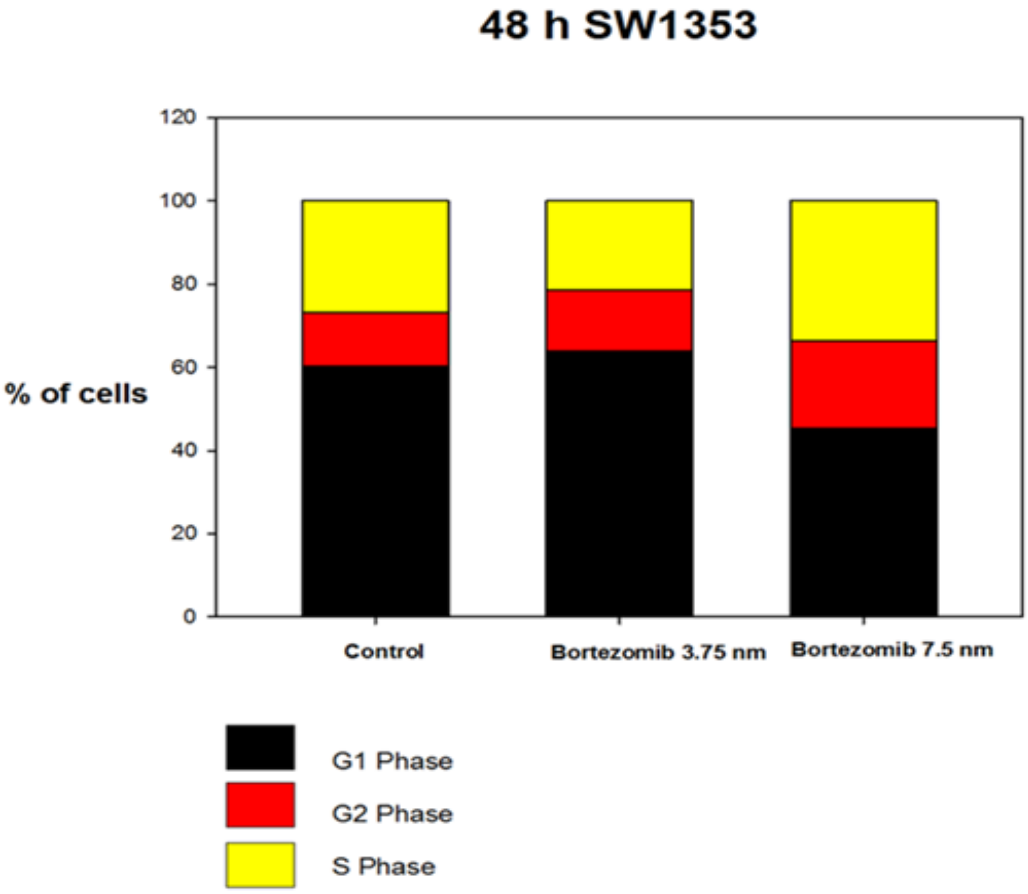

Figure 23: Cell cycle distribution of SW-1353. IC25 and IC50 treatment are shown at the exposure times of 24 h and 48 h

3.6 qPCR

We used qRT-PCR for analyzing the gene expression of the G2/M cell cycle checkpoint genes CDK1, CDK2, cdc25, CCNB, CCNA after IC25 and IC50 treatment. Therefore, we had a qRT-PCR run of 40 repeats. Samples of IC25 and IC50 treatment were compared with a control and the means were performed as bar charts including standard deviation (Figure 24). According to CCNA, the detection of SybrGreen was only possible in the late PCR runs. Consequently, the evaluation of CCNA expression during 40 PCR runs was not possible. Therefore, CCNA data is not shown in Figure 24.

Before the PCR was started, we checked the RIN of the isolated RNA by Agilent 2100 BioAnalyzer. In this respect, we had values between 8.80 and 9.80. Therefore, optimal RIN´s for qRT-PCR could be detected (Table 9).

Isolated RNA/Cntr/IC25/IC50	**RIN - Value**
SW-1353 EX 1 Cntr.	RIN: 8.80
SW-1353 EX 1 IC25	RIN: 9.20
SW-1353 EX 1 IC50	RIN: 8.60
SW-1353 EX 2 Cntr.	RIN: 9.60
SW-1353 EX 2 IC25	RIN: 9.70
SW-1353 EX 2 IC50	RIN: 9.80
SW-1353 EX 3 Cntr	RIN: 8.70
SW-1353 EX 3 IC25	RIN:9
SW-1353 EX 3 IC50	RIN: 9.30
SW-1353 EX 4 Cntr.	RIN: 9.30
SW-1353 EX 4 IC25	RIN: 8.80
SW-1353 EX 4 IC50	RIN: 9.30

Table 9: RIN - Values of isolated RNA

In general, we could observe that the gene expression of CCNB, CDK1, CDK2 and cdc25 was drastically reduced by a treatment of bortezomib. With reference to CCNB, the expression level decreased more than 50 % after IC25 treatment. Interestingly, the decrease was less after IC50 treatment (30 %). CDK1 and cdc25 showed similar behavior. CDK1 - IC25 - value was throttled around 65 % and CDK1 - IC50 - value decreased around 40%. According to cdc25, the IC25 - value falls around 50% and the IC50 - value around 30%.

Only the change of CDK2 expression was in line with our expectations. The gene expression level was influenced in a concentration depending manner. IC25 treatment reduced the expression around 18% and IC50 treatment around 45%.

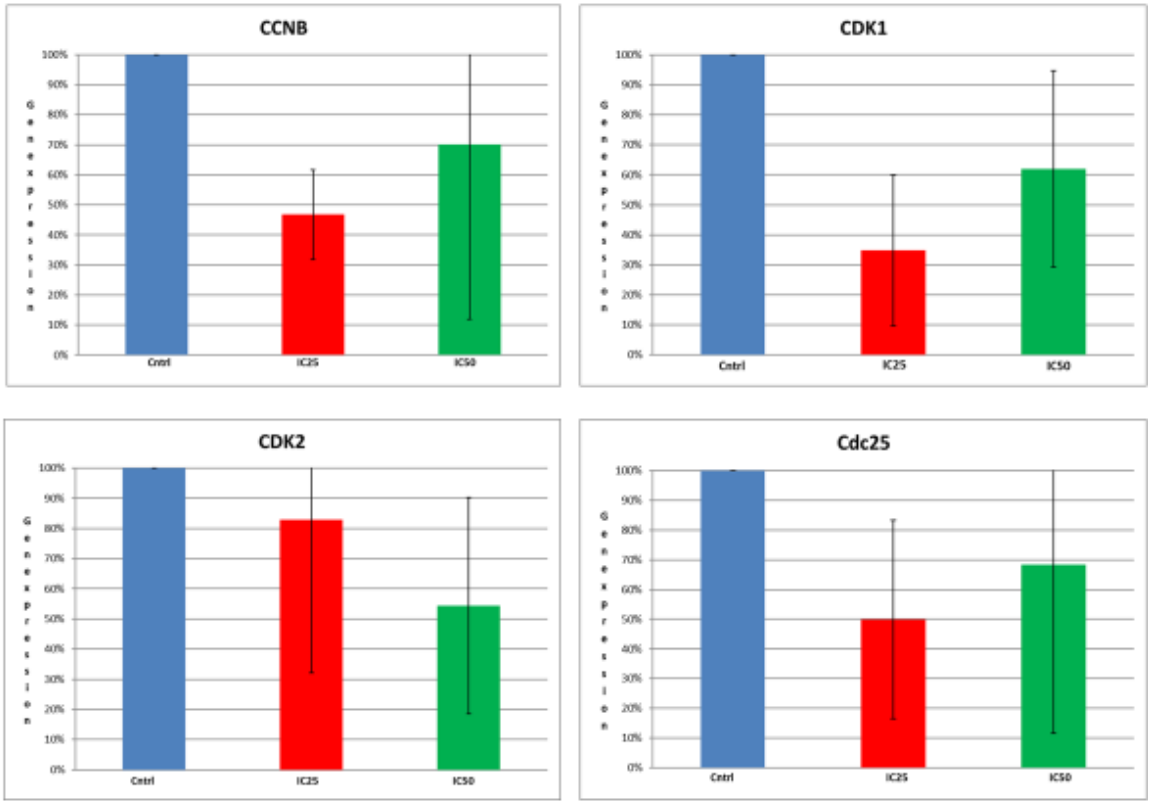

Figure 24: Gene expression levels of CCNB, CDK1, CDK2, cdc25 under the influence of IC25 and IC50 treatment

4 Discussion

The present study was designed to investigate the effect of the proteasome inhibitor bortezomib to chondrosarcoma cells and primary chondrocytes. The idea was generated from earlier studies which reported positive effects of bortezomib to various tumor diseases, for example hepatocellular carcinoma [57], human glioblastoma [58] and multiple myeloma [59]. We also red various publications about the induced G2/M arrest of Bortezomib. [60]

According to the literature, we asked ourselves if there is any effect of bortezomib to chondrosarcoma and if the G2/M arrest is demonstrable including the cyclin/CDK system.

Therefore, the underlying hypothesis was created: The proliferation of chondrosarcoma is inhibited by the proteasome inhibitor bortezomib via the cyclin/CDK system that causes G2/M arrest.

Indeed, the results manifest that the proliferation of chondrosarcoma cells is inhibited by bortezomib, even stronger than the proliferation of healthy chondrocytes. In addition, the effect to tumor cells seems to occur faster.

But in relation to the doses and the course of time, lower concentrations of bortezomib suppress tumor cells for a shorter period than primary chondrocytes. In contrast, higher concentrations throttle the proliferation in both cases.

Referring to the distribution of cell cycle phases, we could demonstrate the significant increase of G2 cells for IC50. This was not possible for IC25. This implies, that the G2/M arrest can only be provoked by higher bortezomib concentrations. We also found significant decrease of S-phase cells and a significant increase of G1-cells. These transitions are controlled by, inter alia, the cyclin/CDK system. Therefore, we checked gene expression levels of CCNA, CCNB, CDK1, CDK2, cdc25. In this process, a general decrease was detectable.

Overall, our hypothesis was largely confirmed by the results. Although, many evaluated experiments show high standard deviation which should be considered with the informative values of this study. Beside pipetting problems, various cell numbers and inaccurate incubation times might be the reason. The MTS experiments should be measured after 2.5 h, but we increased or decreased the incubation time for some experiments depending on the color change. This includes a changing number of cells per well. In addition, sometimes the color change was too high. Therefore, the OD value was no more representative for the metabolic activity. By avoiding these inaccuracies, a dose-

and time-depending decrease of the proliferation should be detectable more impressive. According to the FACS and qRT-PCR results, we must mention that we used a low glucose culture medium by two out of four experiments. This could have influenced the proliferation rate and therefore the cell cycle activity even before the treatment.

Nevertheless, our results can be reconciled with other pre-findings in the literature. Bao et al. also published a dose- and time-depending decrease of chondrosarcoma cell proliferation. The influence of bortezomib to the proliferation of SW-1353 was stronger than to human chondrocytes as well. In contrast to our results, they could also demonstrate that bortezomib treatment mostly leads to G0/G1 arrest including a cyclin D decrease and a smaller downstream of s-phase cells. [26]

Other corresponding data were published by Lohberger et al. They proved the effects of bortezomib to two different cell lines of chondrosarcoma. Even here, a dose- and time depending decrease of the proliferation rate was lockable. According to the SW-1353 cell line, the greatest effects were between 2.5 nm and 25 nm, which is exactly congruent with our results. In conflict with our xCelligence results, a delay in the time-depending proliferation by a treatment of 5 nm bortezomib was not published. The cell index was nearly zero. [61]

Gene expression levels of CDK1, CDK2, cdc25 and CCNB relating to bortezomib and chondrosarcoma are hardly findable in the literature. However, there are a lot of reviews about the effects of bortezomib to other cancer types, which support the idea of disrupting cell cycle regulating mechanism by bortezomib.

Hong et al. published a G2/M-arrest in human colon cancer by using bortezomib. By investigation of G2/M phase-related cell cycle proteins, they could show a hyperactivation of the ataxia telangiectasia mutated/cell cycle checkpoint kinase 1 (ATM/CHK1) pathway. ATM is a serine/threonine kinase which is highly involved in the regulation of DNA damage and repair. Therefore, it is an important switch in case of cell cycle progress. ATM phosphorylates CHK1 and in the following CHK1 conveys a strong DNA-damage signal. They could also demonstrate a simultaneous inactivation of cell division cycle 2 (Cdc2) by phosphorylation through ATM. [62] Cdc2 is part of the cell cycle progress and is also known as CDK1. This is aligned with our study, because we found a downstream of cdk1 in chondrosarcoma cells, too. This also confirms our determined downstream of cdc25 and CCNB. CCNB is only needed for the complex of cyclin B/CDK1 and cdc25 is an important activator of this complex.

Another paper was published by Baiz et al. They investigated the effects of bortezomib in relation to the hepatocellular carcinoma. Beside an increase of G2/M-phase and a decrease of S-phase cells, they reported a decrease of the transcription factor E2F. E2F is indispensable for the transcription of cyclin D1, cyclin A2 and CDK2 for which they could show a general reduction in the gene expression levels. [63] We also found relevant data for the chondrosarcoma. CDK2 was downregulated by bortezomib treatment as well.

In summary, our results support the idea of bortezomib as an inhibitor of the cyclin/CDK system in human chondrosarcoma. We cannot say whether bortezomib directly blocks the cyclin/CDK system or whether another mechanism is responsible for the downstream of CCNA, CCNB, CDK1, CDK2, and cdc25. Other studies included, there are many indications that suggest bortezomib as an inhibitor of pathways which are important for tumor proliferation, although the final key is still unknown. Initial successful applications in the therapy of multiple myeloma and promising approaches in other tumor types, permit us to hope that bortezomib can be used as a chemical drug for the therapy of human chondrosarcoma in the future.

5 References

[1] Böckler, Denk, Heitz, Moch, Pathologie, 4.Auflage Urban&Fischer Elsevier (2008), S. 167

[2] PD Dr. med. Gernot Jundt, Knochentumoren, (1997) Schweizerische Krebsliga

[3] Böckler, Denk, Heitz, Moch, Pathologie, 4. Auflage Urban&Fischer Elsevier (2008), S.1081

[4] Böckler, Denk, Heitz, Moch, Pathologie, 4. Auflage Urban&Fischer Elsevier (2008), S. 1073f

[5] Skinner, McMahon, Orthopedics, Current Diagnosis & Treatment, 5th Edition, McGraw Hill Education (2014), p.265

[6] Riede, Werner, Schaefer, Allgemeine und Spezielle Pathologie, 5.Auflage Thieme (2004), S.1153

[7] Fletcher, Unni, Mertens, World Health Organization Classification of Tumours, Pathology and Genetics of Tumours of Soft Tissue and Bone, Lyon (2002)

[8] Youssef Darouassi, Mohamed Mliha Touati, Mehdi Chihani, Karim Nadour, Mostapha Boussouga, Haddou Ammar, Brahim Bouaity, Chondrosarcoma metastasis in the thyroid gland: a case report, Journal of medical case reports 8, p.157, (2014)

[9] Dt. Ges. f. Orthopädie und orthopäd. Chirurgie + BV d. Ärzte f. Orthopädie (Hrsg.) Leitlinien der Orthopädie, Dt. Ärzte-Verlag, 2. Auflage, Köln (2002)

[10] Alison, the Cancer Handbook second edition, Wiley (2007), p.741f

[11] Horn, Biochemie des Menschen, 5. Auflage, Thieme (2012), S. 252 – 264

[12] Vermeulen, Van Bockstaele, Berneman, The cell cycle: a rewiew of regulation, deregulation and therapeutic targets in cancer, Cell Proliferation, 36, p. 131-149, (2003)

[13] Norbury, Nurse, Animal cell cycles and their control, Annu. Rev. Biochem., 61, p.441, (1992)

[14] David O. Morgan, Principles of CDK regulation, Nature (1995), 374, p.131

[15] Evans T, Rosenthal ET, Youngblom J, Distel D, Hunt T, Cyclin: a protein specified by maternal mRNA in sea urchin eggst hat is destroyed at each cleavage division, (1983), Cell 33, p.389

[16] Sherr CJ, G1 phase progression: cycling on cue, (1994), Cell 79, p. 551

[17] Ohtsubo M, Theodoras AM, Schumacher J, Roberts JM, Pagano M, Human cyclin E, a nuclear protein essential for the G1-to-S-phase transition, (1995), Mol. Cell Biol. 15, p.2612

[18] Girard F, Strausfeld U, Fernandez A, Lamb NJ, Cyclin A is required for the onset of DNA replication in mammalian fibroblasts, (1991), Cell 67, p. 1169

[19] King RW, Jackson PK, Kirschner MW, Mitosis in transition, (1994), Cell 79, p. 563

[20] Buchkovich K, Duffy LA, Harlow E, the retinoblastoma protein is phosphorylated during specific phases of the cell cycle, (1989), Cell 58, p. 1097

[21] Bradbury EM, Inglis RJ, Matthews HR, Control of cell division by very lysine rich histone (F1) phosphorylation, (1974), Nature 247, p.257

[22] Voitenleitner C, Fanning E, Nasheuer HP, Phosphorylation of DNA polymerase alpha-primase by cyclin A-dependent kinases regulates initiation of DNA replication in vitro, (1997), Oncogene 14, p.1611

[23] Nilsson I, Hoffmann I, Cell cycle regulation by the Cdc25 phosphatase family, (2000), Prog. Cell Cycle Res. 4, p.107

[24] Alberts, Johnson, Lewis, Raff, Roberts, Walter, Molekularbiologie der Zelle, 5. Auflage, Wiley-VCH 2011, S.438-443

[25] Mutschler E, Geisslinger G, Kroemer H, Ruth P, Schäfer-Korting M, Mutschler Arzneimittelwirkungen, Lehrbuch der Pharmakologie und Toxikologie, 9.Auflage, Wissenschaftliche Verlagsgesellschaft mbH Stuttgart (2008), S. 947

[26] Xing Bao, Tingting Ren, Yi Huang, Chongmin, Ren,Kang Yang, Hongliang Zhang, Wei Guo, Bortezomib induces apoptosis and suppresses cell growth and metastasis by inactivation of Stat3 signaling in chondrosarcoma, International Journal of Oncology 50, p. 477-486, (2017)

[27] Mitsiades C, Podar K, Munshi NC, Richardson PG, Anderson KC: Proteasome inhibitor PS-341 abrogates IL-6 triggered signaling cascades via caspase-dependent downregulation of gp130 in multiple myeloma. Oncogene 22: 8386-8393, (2003)

[28] Kao,Chao, Tsai, Chuang, Huang, Chen, Lin, Wang, Wang, Lai, Bortezomib enhances cancer cell death by blocking the autophagic flux through simulating ERK phosphorylation, Cell Death and Disease, 5, (2014)

[29] Characteristics of Human Chondrocytes (Internet, qouted 2017 Jun 21), available from: https://www.cellapplications.com/human-chondrocytes-hc

[30] Characteristics of SW1353 (Internet, qouted 2017 Jun. 21), available from: https://www.lgcstandardsatcc.org/Products/Cells_and_Microorganisms/By_Tissue/Bone/HTB-94.aspx?geo_country=at#characteristics

[31] D. Doenecke, J. Koolman, G. Fuchs, W. Gerok, Biochemie und Pathobiochemie, 15. Auflage, Thieme (2005), S. 383

[32] Butler J.M, Forensic DNA Typing: Biology, Technology, and Genetics of STR Markers. 2nd edition. Elsevier Academic Press New York (2005)

[33] Decription of Cell Titer 96® AQueous One Solution Cell Proliferation Assay (Internet, qouted 2017 Jun. 27), available from: https://at.promega.com/-/media/files/resources/protocols/technical-bulletins/0/celltiter-96-aqueous-one-solution-cell-proliferation-assay-system-protocol.pdf

[34] Technology overview of xCELLigence RTCA DP (Internet, quoted 2017 Jun. 30), Available from: https://www.aceabio.com/product/rtca-dp/

[35] Description of propidium iodide (Internet, qouted 2017 Jul. 03), available from: https://www.thermofisher.com/order/catalog/product/P1304MP

[36] Shapiro, Howard, Practical Flow Cytometry, New York, Alan R. Liss, (1985)

[37] Todd C. Lorenz, Polymerase Chain Reaction: Basic Protocol Plus Troubleshooting and Optimization Strategies, Journal of visualized experiments, (2012)

[38] R. G. Prinn and B. Fegley, Jr., Earth Planet., Sci. Lett. 83, 1, (1987)

[39] J. Lewis, H. Watkins, H. Hartman, R. Prinn, Geol. Soc. Am. Spec. Pap.190, p. 215 (1982)

[40] M. R. Palmer and H. Elderfield, Nature (London) 314, 526, (1985)

[41] D. J. DePaolo and B. L. Ingram, Science 227, 938, (1985)

[42] F. Surlyk and M. B. Johansen, ibid. 223, 1174, (1984)

[43] W. H. Burke et al., Geology 10, 516, (1982)

[44] M. A. Wadleigh, J. Veizer, C. Brooks, Geochim. Cosmochim. Acta 49, 1727, (1985)

[45] D. W. Mittlefehldt and G. W. Wetherill, ibid. 43, 201, (1979)

[46] Lilit Garibyan and Nidhi Avashia, Research Techniques Made Simple: Polymerase Chain Reaction (PCR), J Invest Dermatol., 133(3): e6, (2013)

[47] Real-time PCR Handbook, life technologies ^{TM} (Internet, quoted 2017 Jul 04), available from: http://www.gene-quantification.de/real-time-pcr-handbook-life-technologies-update-flr.pdf

[48] RNeasy Mini Handbook [Internet, qoutet 2017 Jul 05), available from: https://www.qiagen.com/at/resources/resourcedetail?id=14e7cf6e-521a-4cf7-8cbc-bf9f6fa33e24&lang=en

[49] K.L. Manchester, Biotechniques 20, 968–970, (1996)

[50] S.R. Gallagher, P.R. Desjardins, Curr. Protoc. Mol. Biol. 3 (2006) (Appendix)

[51] Agilent RNA 6000 Nano Kit Guide (Internet, quoted 2017 Jul. 06) available from: http://www.agilent.com/cs/library/usermanuals/Public/G2938-90034_RNA6000Nano_KG.pdf

[52] PRODUCT INFORMATION DNase I, RNase-free, Thermo Scientific (Internet, quoted 2017, Jul. 06), available from: https://tools.thermofisher.com/content/sfs/manuals/MAN0012000_DNase_I_RNase free_1UuL_UG.pdf

[53] Description of iScript™ cDNA Synthesis Kit (Internet, quoted 2017, Jul. 07), available from: http://www.bio-rad.com/de-at/product/iscript-cdna-synthesis-kit

[54] SYBR Green Real-Time PCR Master Mixes (Internet, quoted 2017, Jul. 07), available from: http://www.thermofisher.com/at/en/home/life-science/pcr/real-time-pcr/real-time-pcr-reagents/sybr-green-real-time-master-mixes.html?gclid=Cj0KCQjw4vzKBRCtARIsAM3l8ODPPRpZh9NYHQUZm-gk1ZyE37GIomC-7uIQ_VfoTu7XGbULSy8pAJgaAi8DEALw_wcB&s_kwcid=AL!3652!3!77558503092!p!!g!!sybr%20green&ef_id=V@bLUwAAAb0fBmp2:20170707112426:s

[55] SYBR® Green based qPCR (Internet, quoted 2017, Jul. 07) available from: http://www.sigmaaldrich.com/life-science/molecular-biology/pcr/quantitative-pcr/sybr-green-based-qpcr.html

[56] Vandesompele J, De Preter K, Pattyn F, Poppe B, Van Roy N, De Paepe A, Speleman F, Accurate normalization of real-time quantitative RT-PCR data by geometric averaging of multiple internal control genes, Genome Biology (2002)

[57] K. Wahl, M. Siegemund, F. Lehner, F. Vondran, A. Nüssler, F. Länger, T. Krech, R.Kontermann, M. P. Manns, K. Schulze-Osthoff, K. Pfzenmaier, H. Bantel, Increased apoptosis induction in hepatocellular carcinoma by a novel tumor-targeted TRAIL fusion protein combined with Bortezomib, Hepatology, Vol.57, No. 2, (2013)

[58] X. Zhang, W. Li, C. Wang, X. Leng, S. Lian, J. Feng, J. Li, H. Wang, Inhibition of autophagy enhances apoptosis induced by proteasome inhibitor bortezomib in human glioblastoma U87 and U251 cells, Mol. Cell Biochem, 385, p. 265-275, (2014)

[59] Sun CY, Li JY, Chu ZB, Zhang L, Chen L, Hu Y, Efficacy and Safety of Bortezomib Maintenance in Patients with Newly Diagnosed Multiple Myeloma: A Meta-Analysis, Bioscience reports, (2017)

[60] G. Lu, V. Punj, P. M. Chaudhary, Proteasome inhibitor Bortezomib induces cell-cycle arrest and apoptosis in cell lines derived from Ewing's sarcoma family of tumors and synergizes with TRAIL, Cancer Biology & Therapy, (2008)

[61] Birgit Lohberger, Bibiane Steinecker-Frohnwieser, Nicole Stuendl, Heike Kaltenegger, Andreas Leithner, Beate Rinner, The Proteasome Inhibitor Bortezomib Affects Chondrosarcoma Cells via the Mitochondria-Caspase Dependent Pathway and Enhances Death Receptor Expression and Autophagy, PLoS ONE, (2016)

[62] Y. Hong, S. Hong, S. KIM, D. JIN, J. Shin, D. Yoon, K. KIM, J. LEE, D.HEO, J. LEE, T. KIM, Bortezomib induces G2-M arrest in human colon cancer cells through ROS-inducible phosphorylation of ATM-CHK1, International Journal of oncology 41, p. 76-82, (2012)

[63] Baiz D, Pozzato G, Dapas B, Farra R, Scaggiante B, Grassi M, Uxa L, Giansante C, Zennaro C, Guarnieri G, Grassi G, Bortezomib arrests the proliferation of hepatocellular carcinoma cells HepG2 and JHH6 by differentially affecting E2F1, p21 and p27 levels, Biochimie,91(3), p.373-82, (2009)